Pulses in singularly perturbed reaction-diffusion systems

Veerman, F.W.J.

2

Pulses in a slowly nonlinear Gierer-Meinhardt equation

The content of this chapter was published as [54].

2.1 Introduction

The study of localised pulses in a two-component system of singularly perturbed reaction-diffusion equations has been a very active field of research since the nineties of the previous century. In its most general form, a system that may exhibit such a pulse reads – in one, unbounded, spatial dimension –

$$\begin{cases} U_t = \quad U_{xx} + F(U,V) & \text{(2.1a)} \\ V_t = \varepsilon^2 V_{xx} + G(U,V) & \text{(2.1b)} \end{cases}$$

with $U, V : \mathbb{R} \times \mathbb{R}^+ \to \mathbb{R}$, and $0 < \varepsilon \ll 1$ asymptotically small. The nonlinear reaction terms $F, G : \mathbb{R}^2 \to \mathbb{R}$ are assumed to satisfy $F(\bar{U}, \bar{V}) = G(\bar{U}, \bar{V}) = 0$ for certain $(\bar{U}, \bar{V})$, such that the trivial background state $(U, V) \equiv (\bar{U}, \bar{V})$ is spectrally stable. However, research on pulses in equations of the type (2.1) has been restricted mostly to model equations. In particular two of these models have played a central role in the development of the theory: the (irreversible) Gray-Scott (GS) equation for a class of autocatalytic reactions [23] – that became the centre of research attention by the intriguing observations in [38, 43] – and the Gierer-Meinhardt (GM) equation [22] for (biological) morphogenesis – for which the existence problem has already been

considered in the mathematical literature for a somewhat longer time [48]. For both the GS and the GM model, quite precise insight has been obtained in the existence, stability and dynamics of localised (multi-) pulses, also in more than one spatial dimension – although one certainly cannot claim that the models are fully understood; see [5, 6, 7, 12, 13, 26, 32, 33, 34, 41, 42, 51, 58] and the references therein for the literature on one spatial dimension.

The 'fast' V-component of a localised (multi)pulse solution of a singularly perturbed model (2.1) is asymptotically localised: it decays exponentially to the V-component $\bar{V}$ of the background state on a spatial scale that is asymptotically shorter than the spatial scale associated to the 'slow' U-component. As a consequence, the two-component (U, V)-flow generated by (2.1) is governed by a scalar equation in the slow component U:

$$U_t = U_{xx} + F(U, \bar{V}) \tag{2.2}$$

except for the asymptotically small spatial regions in which the V-component is not exponentially close to $\bar{V}$. Clearly, this is in general a nonlinear equation. However, for the GS and GM models, this slow reduced scalar equation is linear:

$$\begin{array}{lll} \text{(GS)} & U_t = U_{xx} + A(1-U), & A > 0 \text{ parameter}, \quad (\bar{U}, \bar{V}) = (1, 0) \\ \text{(GM)} & U_t = U_{xx} - \alpha U, & \alpha > 0 \text{ parameter}, \quad (\bar{U}, \bar{V}) = (0, 0) \end{array} \tag{2.3}$$

In fact, as far as we are aware, this – the fact that the counterpart of (2.2) is linear – is the case for all singularly perturbed two-component reaction-diffusion equations with exponentially localised pulse solutions considered in the literature (including the Schnakenberg model [46, 56]). There are a number of papers in the literature in which more general classes of equations than the GS or GM models are considered – see [4, 6, 10]. In these papers the background state $(\bar{U}, \bar{V})$ is translated to $(0, 0)$ so that $F(\bar{U}, \bar{V}) = F(0, 0) = 0$ in (2.1). Moreover, the nonlinear part of $F(U, V)$ is assumed to be separable, i.e. $F(U, V)$ is written as $-\alpha U + F_1(U)F_2(V)$. Therefore $F_2(\bar{V}) = F_2(0) = 0$, and these more general systems also reduce to linear slow scalar equations like (2.3) outside the asymptotically small regions where V is not close to $\bar{V}$.

In this chapter, and in the subsequent chapter 3, we consider the potential impact of the nonlinearity of $F(U, \bar{V})$ as function of U in comparison with the literature on 'slowly linear' model systems such as GS and GM. Here, we consider a very explicit model problem, a Gierer-Meinhardt equation with a 'slow nonlinearity' (see (2.7) below), in full analytical detail; in chapter 3, we consider the existence and stability

of pulses in a general setting, i.e. as solutions of (2.1). We refer to Remark 2.1 for a more specific motivation of our choice to study equations with 'slow nonlinearities'.

In the standard form (2.1), the classical Gierer-Meinhardt equation [22] is given by

$$\begin{cases} U_t = \quad U_{xx} - \alpha\, U + \sigma\, V^2 & \text{(2.4a)} \\ V_t = \varepsilon^2 V_{xx} - V + \dfrac{V^2}{U} & \text{(2.4b)} \end{cases}$$

in which $\alpha > 0$ is the main bifurcation parameter and $\sigma > 0$ is most often scaled to 1. The pulse type solutions of (2.4) have an amplitude of $O\left(\frac{1}{\varepsilon}\right)$ [6, 26]. Therefore, we scale U and V and subsequently x and ε,

$$U \to \frac{U}{\varepsilon},\ V \to \frac{V}{\varepsilon},\ x \to \sqrt{\varepsilon}\, x,\ \varepsilon \to \varepsilon^2 \tag{2.5}$$

to bring (2.4) in its 'normal form' [6]

$$\begin{cases} \varepsilon^2 U_t = \quad U_{xx} - \varepsilon^2 \alpha\, U + \sigma\, V^2 & \text{(2.6a)} \\ \quad V_t = \varepsilon^2 V_{xx} - V + \dfrac{V^2}{U}. & \text{(2.6b)} \end{cases}$$

In this chapter, we study a 'slowly nonlinearised' version of (2.6), that is obtained from (2.6) by adding a very simple nonlinear term to its 'slow' U-equation (2.6a):

$$\begin{cases} \varepsilon^2 U_t = \quad U_{xx} - \varepsilon^2 \left(\alpha\, U - \gamma\, U^d\right) + \sigma\, V^2 & \text{(2.7a)} \\ \quad V_t = \varepsilon^2 V_{xx} - V + \dfrac{V^2}{U} & \text{(2.7b)} \end{cases}$$

with new parameters $\gamma \geq 0$, $d > 1$. Moreover, we now allow $\sigma \in \mathbb{R}\backslash\{0\}$. Systems incorporating such a slow nonlinearity were already encountered in [37] (although no pulse type solutions were considered in this paper). This equation indeed reduces to a nonlinear slow reduced scalar U-equation away from the regions in which V is not exponentially close to $\bar{V} = 0$:

$$U_t = U_{\chi\chi} - \alpha\, U + \gamma\, U^d \tag{2.8}$$

in which $\chi = \varepsilon x$ is a 'super-slow' spatial coordinate – see section 2.2. Note that scaling back the additional 'slowly nonlinear' term $\gamma\, U^d$ through (2.5) introduces an $O\left(\varepsilon^{d-1}\right)$, i.e an asymptotically small, additional term to the Gierer-Meinhardt equation in its classical form (2.4). We will see in the upcoming analysis that this term has

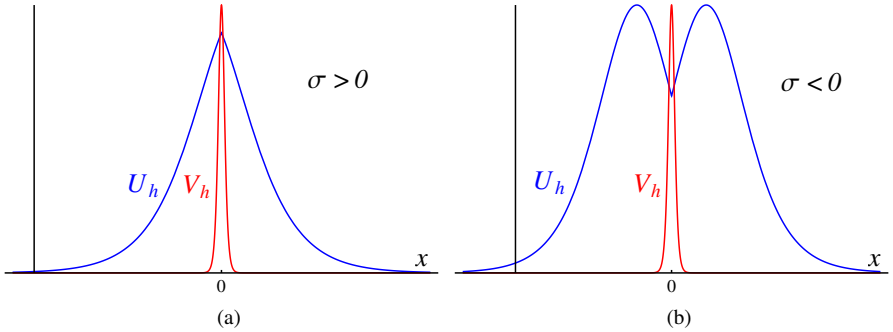

Figure 2.1: The stationary homoclinic pulse $(U_h(x), V_h(x))$ of (2.7); (a) $\sigma > 0$, (b) $\sigma < 0$.

a significant impact on the dynamics generated by (2.4). Thus, in a way, our work can also be interpreted as a study of the 'vulnerability' of the classical Gierer-Meinhardt model (2.4) to asymptotically small 'slowly nonlinear' changes to the model.

In recent years, the analysis of localised pulses in one-dimensional singularly perturbed reaction-diffusion equations has been focused mostly on pulse dynamics and interactions – see [5, 10, 12, 34] and the references therein. However – like the work on multi-pulse patterns [26, 32, 33, 51, 52, 56] – this analysis is based on fundamental insights on the existence and stability of stationary, solitary, pulses [6, 7, 13, 48, 58]. On the unbounded domain, i.e. for $x \in \mathbb{R}$, these pulses correspond to homoclinic solutions of the four-dimensional spatial dynamical system reduction of the partial differential equation. Here, we restrict our analysis to the existence and stability of homoclinic stationary pulse solutions $(U_h(x), V_h(x))$ to (2.7) that are bi-asymptotic to the background state $(0, 0)$, i.e. $\lim_{x\to\pm\infty}(U_h(x), V_h(x)) = (0, 0)$. Especially the issue of stability requires a significant extension of the methods developed in the literature for 'slowly linear' GS/GM-type models. The present results form the foundation for a subsequent analysis of the multi-pulse patterns – see remark 2.1 – and pulse interactions. Moreover, already at the level of these most basic pulse solutions, we encounter novel phenomena in the dynamics generated by (2.7) that have not yet been observed in the literature on 'slowly linear' models.

The existence problem – see section 2.2 – can be studied directly along the lines developed in [6] for 'slowly linear' normal form models of GM type with a separable

nonlinearity. Our main result on the existence of homoclinic pulses $(U_h(x), V_h(x))$, Theorem 2.2, can be established by a direct application of the methods of geometric singular perturbation theory [18, 19]. In other words, at the existence level the 'slow nonlinearity' in (2.7) does not require the development of novel theory. However, it is established by Theorem 2.2 that (2.7) does exhibit homoclinic pulse patterns that differ significantly from those found in 'slowly linear' GS/GM-type models. Unlike linear slow reductions such as (2.3), the planar stationary problem associated to reduction (2.8) has orbits homoclinic to its saddle point (that corresponds to the background state of (2.7)). As a consequence, unlike the classical GM model (2.4), system (2.7) has homoclinic pulse solutions $(U_h(x), V_h(x))$ for $\sigma < 0$. At leading order in ε, the slow U-component $U_h(x)$ follows a large part of the homoclinic orbit of (2.8), so that for $\sigma < 0$ the slow component of the solitary homoclinic 1-pulse solution has the leading order structure of two combined slow scalar pulses – see Figure 2.1b.

The spectral stability of $(U_h(x), V_h(x))$ is studied in section 2.3 by the Evans function $\mathcal{D}(\lambda)$ associated to the linearised stability problem, following the ideas developed in [6, 7]. As is to be expected from the general theory [3], $\mathcal{D}(\lambda)$ can be decomposed into a slow and a fast component, and all nontrivial eigenvalues are determined by the slow component. In [6, 7], i.e. for the GM and GS models, the zeroes of this slow component are determined analytically by 'the NLEP method'. The linearity of the slow scalar reduction (2.3) plays a central role in this approach – as it does in all analytical studies of the spectral stability of pulses in GS/GM-type models (see [5, 26, 32, 33, 34, 51, 58] and the references therein). More explicitly, the fact that the spectral stability problem is exponentially close to a constant coefficients eigenvalue problem outside the asymptotically small regions in which V is not close to $\bar{V}$ is a crucial ingredient of the stability analysis of GS/GM-type models. Due to the nonlinearity in the slow scalar reduction (2.8) this is not the case for (2.7): away from the fast V-pulse, the linear operator associated to the stability problem still has coefficients that depend explicitly (and slowly) on x (on χ – see (2.8)). Its solution space is therefore not governed by simple, pure exponentials (as for GS/GM-type models).

The key to the NLEP approach as developed in [6, 7] is constructing a set of basis functions for the linear operator/system associated to the stability of the pulse for which the Evans function $\mathcal{D}(\lambda)$ – the determinant of this set – can be evaluated, or better: approximated, explicitly. In chapter, and in the subsequent chapter 3, we show that the NLEP approach can be based on a set of basis functions that is determined by the slowly varying problem outside the fast V-pulse region, in such a way that it is still possible to determine an analytical approximation for the zeroes of $\mathcal{D}(\lambda)$.

Here, a central role is played by the χ-dependent Sturm-Liouville problem associated to the linearisation of (2.8) about its (stationary) homoclinic orbit, defined on a half-line. This problem has a two-dimensional set of slowly varying solutions. We show that these solutions can take over the role of the slow exponentials coming from the (slow) stability problem about the trivial state $U = 0$ of the linear constant coefficient GS/GM-type reductions (2.3). In the context of this chapter, these solutions can be expressed in terms of Legendre functions, due to the special/simple nature of the nonlinearity in (2.8). In the general setting of chapter 3, the construction of the Evans functions cannot be this explicit. The main novel analytical result of this chapter is given by Theorem 2.12, in which indeed an explicit expression is given for the zeroes of $\mathcal{D}(\lambda)$, which is a generalisation of the corresponding 'slowly linear' results in [6, 7].

In section 2.4, we analyse and interpret the expression obtained in Theorem 2.12. One of our first – and quite straightforward – results is Corollary 2.15: the $\sigma < 0$ 'double hump' pulses of Figure 2.1b cannot be stable. The $\sigma > 0$ pulses of Figure 2.1a, however, can very well be stable. In Figure 2.3, a graphical description is given of our two main stability results, Theorems 2.18 and 2.19. The stability of the pulse $(U_h(x), V_h(x))$ depends strongly on the character of the 'slow nonlinearity' in (2.7). As long as the exponent of the nonlinearity d is smaller than 3, the stability scenario is exactly like that of the 'slowly linear' GS/GM-type models: $(U_h(x), V_h(x))$ stabilises by a Hopf bifurcation for increasing α – even the shape of the orbit of the critical eigenvalues $\lambda(\alpha)$ through $\mathbb{C}$ is very similar to its counterparts in [6, 7]. However, this orbit changes drastically when d becomes larger than 3 – see Figure 2.3: for $d > 3$ there is a second Hopf bifurcation (as function of α) that destabilises $(U_h(x), V_h(x))$. Different from the results on GS/GM-type models, for $d > 3$, there is only a bounded α-region for which $(U_h(x), V_h(x))$ can be stable. In Theorem 2.20 this is established rigorously for $d > 3$ large enough.

Finally, in section 2.5, we present some simulations of (2.7). We have not attempted to perform a systematic (numerical bifurcation) analysis of the dynamics of (2.7). Apart from checking (and confirming) the outcome of our asymptotic stability analysis, our goal has been to obtain an indication of whether or not the 'slow nonlinearity' of (2.7) generates behaviour that is not known from the (vast) literature on GS/GM-type models.

We are not aware of any examples in the literature on GS/GM-type models of stable non-moving solitary pulses that are not completely stationary. A priori, one

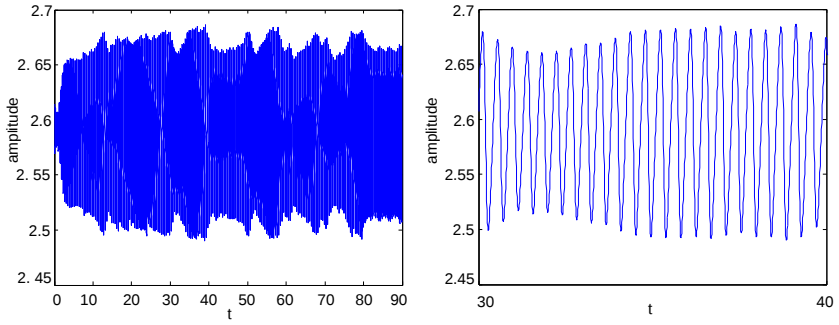

(a) (b)

Figure 2.2: The dynamics of the maximum of the U-pulse as function of time in a simulation of (2.7) with $\gamma = 2$, $\sigma = 1$, $\varepsilon = 0.002$, $d = 5$ and $\alpha = 90.6$ for $x \in [-5000, 5000]$ with homogeneous Neumann boundary conditions – (b) zooms in on a small part (in time) of (a). The position of the maximum does not vary in time. The value of α is close to the second Hopf bifurcation at which $(U_h(x), V_h(x))$ destabilises – see Figure 2.3.

would expect that if a pulse is destabilised (for instance by decreasing α in the GM model (2.4)), it may bifurcate into a stable standing pulse with a periodically varying amplitude. However, this requires a supercritical Hopf bifurcation, and all Hopf bifurcations of stationary pulses in GS/GM-type models reported on in the literature seem to be subcritical: as α decreases through its critical Hopf bifurcation value, the standing pulse starts to oscillate up and down, but the amplitude of this oscillation grows and after a certain time the pulse is extinguished – see for instance Figure 2.11 (a) in section 2.5. It should be noted that this statement is based on numerical observations, the nature of the Hopf bifurcation of solitary, standing pulses in GS/GM-type models has not been analysed in the literature (for instance by a centre manifold reduction). Moreover, it should also be remarked that – for instance – the GS model does exhibit periodic and even chaotic pulse dynamics – see for instance [5, 42]. However, this richer type of behaviour occurs only in the context of pulse interactions, it is governed by the interactions between travelling pulses, and/or between pulses and the boundary of the domain. We have not considered this type of dynamics here, as we have completely focused on the behaviour of standing, solitary spatially homoclinic pulses. Nevertheless, we have observed very rich dynamics, much richer

than that exhibited by linear GS/GM-type models. In section 2.5 examples are given of periodically oscillating pulses, i.e. standing pulses with an amplitude that varies periodically in time; quasi-periodically oscillating pulses – the amplitude of the pulse oscillation is modulated periodically – and oscillating pulses of which the amplitude is modulated in an even more complex fashion. A simulation of such a 'chaotically oscillating pulse' is shown in Figure 2.2.

In this chapter, it is not investigated whether the pulse dynamics of Figure 2.2 is 'chaotic' or –for instance– is quasi-periodic with three or more independent frequencies. In other words, we do not study the details of the associated bifurcation scenario and do not compute any measure by which the (possible) chaotic nature of the pulse dynamics can be quantified. The analytic core of this chapter, the analysis of the spectrum associated to the stability of $(U_h(x), V_h(x))$, serves as an ideal starting point for a centre manifold analysis of the nature of the Hopf (and subsequent) bifurcations for pulses and/or multi-pulses occurring in this model (and/or generalisations of (2.7)). This will be the subject of chapter 4, where analytic insight in (the possible route leading to) the complex/chaotic behaviour observed in Figure 2.2 will be obtained.

Remark 2.1. Our research is strongly motivated by recent findings on the character of the destabilisation of spatially periodic multi-pulse patterns with long wavelength L. In [52] it is established for GM-type models that these patterns can only be destabilised by two distinct types of Hopf bifurcations as $L \to \infty$, one in which the linearly growing mode also has wavelength L – the most commonly encountered destabilisation in the literature – and another in which this mode has wavelength $2L$. Moreover, these destabilisations alternate countably many times as $L \to \infty$. This is called the 'Hopf dance' in [52]. This Hopf dance also occurs in the GS model, as indicated by the AUTO-simulations in [52]. The GM analysis in [52] shows that this 'dance' is completely driven by the exponential expression $E(L) = e^{-L\sqrt{\alpha+\lambda_h}}$ associated to the slow reduced eigenvalue equation $u_{xx} - \alpha u = \lambda_h u$ originating from (2.3), in which $\lambda_h \in \mathbb{C}$ is the (complex) eigenvalue of the homoclinic ($L \to \infty$) limit pattern. The rotation of $E(L) \in \mathbb{C}$ as $L \to \infty$ is the mechanism underpinning the Hopf dance. From a generic point of view, it is not at all clear why this 'linear' Hopf dance should take place (this is even more obvious for the subsequent 'belly dance' [52]). Hence, to really understand the subtleties involved in the destabilisation of long wavelength spatially periodic patterns, one needs to go beyond 'slowly linear' models for which the associated 'slow reduced' eigenvalue problems are not governed by expressions as $E(L)$. In other words, one needs to study systems of the type (2.1) with $F(U, \bar{V})$ not linear as a function of U.

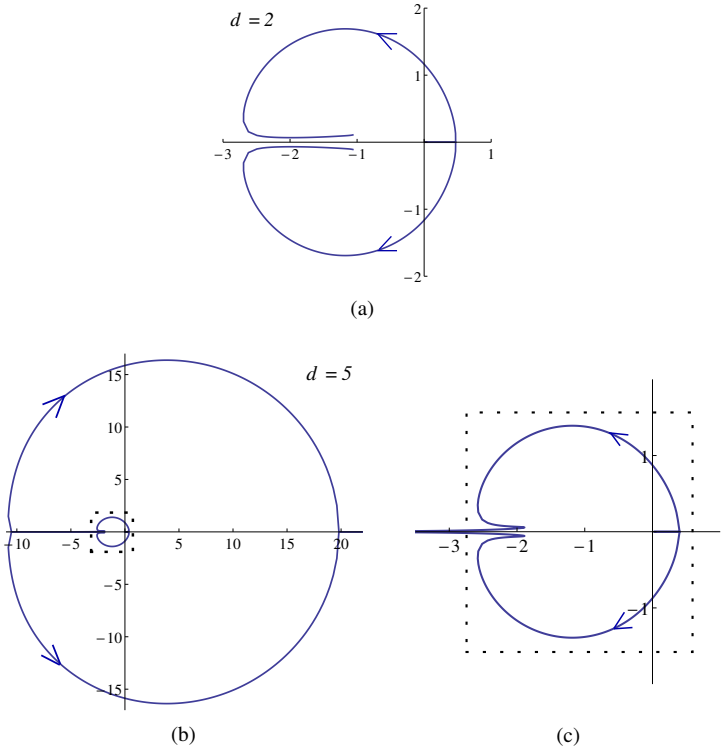

(a) (b) (c)

Figure 2.3: The orbits through $\mathbb{C}$ of the critical eigenvalue λ associated to the spectral stability of $(U_h(x), V_h(x))$ as function of increasing α ($\gamma = 2$, $\sigma = 1$), to leading order in ε. (a) $d = 2 < 3$: The same scenario as in the GS and the GM models [6, 7]. Two real positive eigenvalues merge and become a pair of complex conjugate eigenvalues that travels through the imaginary axis: the pulse is stabilised by a Hopf bifurcation at a critical value of α. (b) $d = 5 > 3$: A significantly different scenario. The eigenvalues initially display the same behaviour as in the case $d < 3$: the pulse is again stabilised by a Hopf bifurcation. However, for α increasing further, the orbits sharply turn around and follow the imaginary axis closely in the negative direction – see (c), a zoom of (b). Eventually, the orbits branch off, head back to the imaginary axis, and again cross the imaginary axis at a second critical – Hopf – value of α. Finally, the pair meets again at the positive real axis and splits up into two positive real valued eigenvalues.

2.2 Pulse construction

Our goal is to construct a stationary pulse solution which is homoclinic to the trivial background state $(U, V) = (0, 0)$. To achieve this goal, we use the singularly perturbed nature of the system. The spatial dynamics of the stationary pulse are given by the four-dimensional system

$$\begin{cases} u_x = p & \text{(2.9a)} \\ p_x = -\sigma v^2 + \varepsilon^2 \left(\alpha u - \gamma u^d\right) & \text{(2.9b)} \\ \varepsilon v_x = q & \text{(2.9c)} \\ \varepsilon q_x = v - \dfrac{v^2}{u} & \text{(2.9d)} \end{cases}$$

Along the lines of Fenichel theory, we can perform a slow-fast decomposition in the spatial variable x: recognising system (2.9) as the *slow* system, we can define the fast variable $\xi = \frac{x}{\varepsilon}$ to obtain the associated *fast* system

$$\begin{cases} u_\xi = \varepsilon p & \text{(2.10a)} \\ p_\xi = -\varepsilon \sigma v^2 + \varepsilon^3 \left(\alpha u - \gamma u^d\right) & \text{(2.10b)} \\ v_\xi = q & \text{(2.10c)} \\ q_\xi = v - \dfrac{v^2}{u} & \text{(2.10d)} \end{cases}$$

The trivial background state is in these systems represented by the origin $(u, p, v, q) = (0, 0, 0, 0)$. While the vector field which generates the flow of the system is not defined at the origin due to the singular $\frac{v^2}{u}$ term in the v-equation, the ratio $\frac{v^2}{u}$ will be well-defined for the constructed pulse.

2.2.1 Geometric analysis

When $\varepsilon \to 0$, the slow and fast systems (2.9) and (2.10) reduce to the *reduced slow system*

$$u_{xx} = -\sigma v^2 \quad \text{(2.11a)}$$

$$q = v - \frac{v^2}{u} = 0 \quad \text{(2.11b)}$$

and the *reduced fast system*

$$u_\xi = p_\xi = 0 \tag{2.12a}$$

$$v_{\xi\xi} = v - \frac{v^2}{u} \tag{2.12b}$$

We see that in this limit, the slow and fast dynamics decouple completely. We define $\mathcal{M}_0 = \{(u, p, v, q) \,|\, u > 0,\ v = q = 0\}$ as the two-dimensional normally hyperbolic invariant manifold that consists of hyperbolic equilibria of the reduced fast system (2.12); it has three-dimensional stable and unstable manifolds $\mathcal{W}^{\mathrm{s,u}}(\mathcal{M}_0)$ which are the unions of the two-parameter families of one-dimensional stable and unstable manifolds (fibres) at the saddle points $(u_0, p_0, 0, 0) \in \mathcal{M}_0$. The reduced fast dynamics (2.12) allow a two-parameter family of homoclinic solutions $v_{0,h}$:

$$v_{h,0}(\xi; u_0, p_0) = \frac{3\,u_0}{2}\,\mathrm{sech}^2\left(\tfrac{1}{2}\xi\right) \tag{2.13}$$

The union over this family as a bundle over $\mathcal{M}_0$ forms the intersection $\mathcal{W}^{\mathrm{s}}(\mathcal{M}_0) \cup \mathcal{W}^{\mathrm{u}}(\mathcal{M}_0)$, see Figure 2.4a.

Fenichel persistence theory [18, 19, 29, 30] states that, for ε sufficiently small, the full system (2.10) has a locally invariant slow manifold $\mathcal{M}_\varepsilon$ which is $O(\varepsilon)$ close to $\mathcal{M}_0$. Since $\mathcal{M}_0$ is also invariant under the non-reduced (fast) flow of (2.10), we have already found $\mathcal{M}_\varepsilon = \mathcal{M}_0$. Moreover, Fenichel theory states the existence of three-dimensional stable and unstable manifolds $\mathcal{W}^{\mathrm{s,u}}(\mathcal{M}_\varepsilon)$ which are $O(\varepsilon)$ close to their unperturbed counterparts $\mathcal{W}^{\mathrm{s,u}}(\mathcal{M}_0)$. The intersection $\mathcal{W}^{\mathrm{s}}(\mathcal{M}_\varepsilon) \cap \mathcal{W}^{\mathrm{u}}(\mathcal{M}_\varepsilon)$ exists, is transversal and therefore determines a two-dimensional manifold. This existence and transversality is based on a Melnikov-type calculation in [6], which can be applied directly to system (2.10). Since the original model equations (2.7) are invariant under reflection in the spatial variable $x \to -x$, this reflection is in the four-dimensional system (2.9) equivalent to the momentum reflection $(p, q) \to (-p, -q)$. Because the coordinate reflection $\xi \to -\xi$ maps $\mathcal{W}^{\mathrm{s}}(\mathcal{M}_\varepsilon)$ to $\mathcal{W}^{\mathrm{u}}(\mathcal{M}_\varepsilon)$ and vice versa, it follows that the intersection of these two manifolds is symmetric in the invariant subset of the momentum reflection, the two-dimensional hyperplane $\{(u, p, v, q) \,|\, p = q = 0\}$. The transversality of this hyperplane to $\mathcal{M}_\varepsilon$ excludes the possibility that it has the intersection $\mathcal{W}^{\mathrm{s}}(\mathcal{M}_\varepsilon) \cap \mathcal{W}^{\mathrm{u}}(\mathcal{M}_\varepsilon)$ as a subset, from which we can conclude that $\mathcal{W}^{\mathrm{s}}(\mathcal{M}_\varepsilon) \cap \mathcal{W}^{\mathrm{u}}(\mathcal{M}_\varepsilon)$ intersects the hyperplane $\{(u, p, v, q) \,|\, p = q = 0\}$ transversally. This determines a one-parameter family of orbits bi-asymptotic to $\mathcal{M}_\varepsilon$. Since both $\mathcal{W}^{\mathrm{s}}(\mathcal{M}_\varepsilon)$ and $\mathcal{W}^{\mathrm{u}}(\mathcal{M}_\varepsilon)$ are $O(\varepsilon)$ close to $\mathcal{W}^{\mathrm{s,u}}(\mathcal{M}_0)$ where the two-parameter family of homoclinic orbits was parametrised by u_0 and p_0 (see (2.13)), it is convenient to

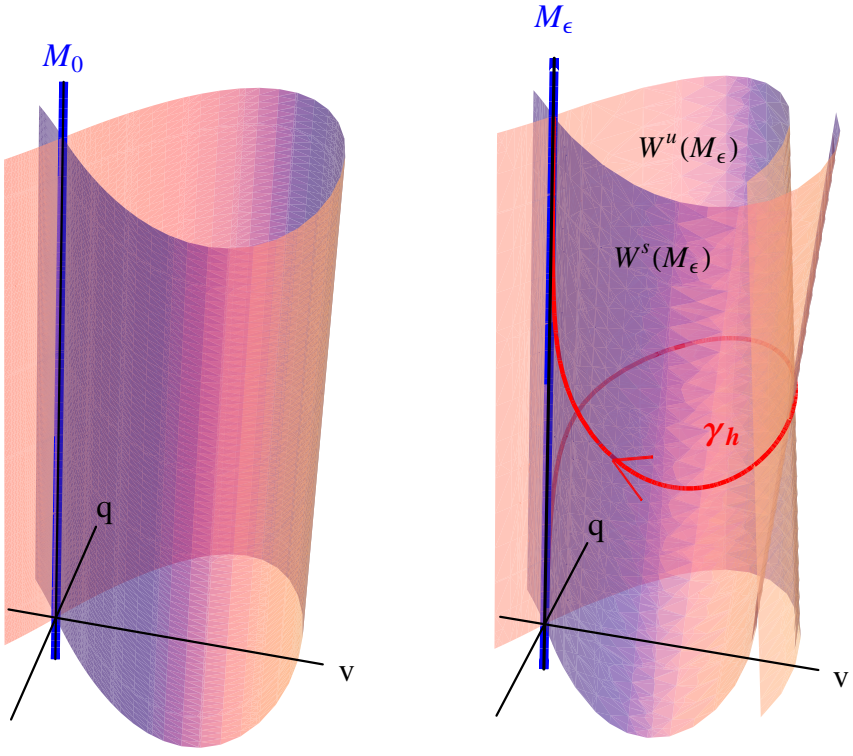

(a) (b)

Figure 2.4: Transversal intersection of the stable and unstable manifolds. (a): The family of homoclinic orbits $v_{h,0}(\xi; u_0, p_0)$, viewed as a bundle over $\mathcal{M}_0$. Both u- and p-directions are along the vertical axis; $\mathcal{M}_0$ is indicated in blue. (b): For the perturbed system ($\varepsilon > 0$), $\mathcal{W}^{\mathrm{s}}(\mathcal{M}_\varepsilon)$ and $\mathcal{W}^{\mathrm{u}}(\mathcal{M}_\varepsilon)$ intersect transversally: γ_h (indicated in red) represents $\mathcal{W}^{\mathrm{s}}(\mathcal{M}_\varepsilon) \cap \mathcal{W}^{\mathrm{u}}(\mathcal{M}_\varepsilon)$, a one-parameter family of orbits homoclinic to $\mathcal{M}_\varepsilon$ – recall that $\dim(\mathcal{M}_\varepsilon) = 2$, $\dim(\mathcal{W}^{\mathrm{s,u}}(\mathcal{M}_\varepsilon)) = 3$ so $\dim(\gamma_h) = 2$.

use u_0 to parametrise the one-parameter family of orbits bi-asymptotic to $\mathcal{M}_\varepsilon$ determined by $\mathcal{W}^{\mathrm{s}}(\mathcal{M}_\varepsilon) \cap \mathcal{W}^{\mathrm{u}}(\mathcal{M}_\varepsilon)$. For a sketch of the situation, see Figure 2.4b.

The next step is to use this structure to construct an orbit homoclinic to $(0,0,0,0)$ in the full, perturbed system (2.9) / (2.10). For that purpose, it is necessary to consider the dynamics on $\mathcal{M}_\varepsilon$. The flow on $\mathcal{M}_\varepsilon$ can be determined by substituting $v = q = 0$ in (2.9) and yields

$$u_{xx} = \varepsilon^2 \left(\alpha\, u - \gamma\, u^d \right) \tag{2.14}$$

Introducing a super-slow coordinate $\chi = \varepsilon x$, this can be written as

$$u_{\chi\chi} = \alpha\, u - \gamma\, u^d \tag{2.15}$$

This equation allows a solution (bi)asymptotic to the trivial background state: since $\gamma > 0$, it is homoclinic to $(0,0,0,0) \in \mathcal{M}_\varepsilon$ and explicitly given by

$$u_{h,0}(\chi) = \left[\frac{\alpha(d+1)}{2\gamma} \operatorname{sech}^2 \left(\tfrac{1}{2}(d-1)\sqrt{\alpha}\chi \right) \right]^{\frac{1}{d-1}} \tag{2.16}$$

The super-slow dynamics on $\mathcal{M}_\varepsilon$ allows us to get a grip on picking exactly that orbit bi-asymptotic to $\mathcal{M}_\varepsilon$ from the intersection $\mathcal{W}^{\mathrm{s}}(\mathcal{M}_\varepsilon) \cap \mathcal{W}^{\mathrm{u}}(\mathcal{M}_\varepsilon)$ which is also homoclinic to $(0,0,0,0) \in \mathcal{M}_\varepsilon$, that is, which is -mostly- asymptotically close to $u_{h,0} \in \mathcal{M}_\varepsilon$. This orbit will make a *fast* excursion through the V-field, since this is where the fast dynamics take place (see (2.10), (2.12)). Since our goal is to construct a symmetric pulse, we can choose an interval symmetric around the origin in which the fast jump occurs. The interval needs to be asymptotically small with respect to the slow variable x, but asymptotically large with respect to the fast variable ξ: to be asymptotically close to $\mathcal{M}_\varepsilon$, the V-component of the pulse needs to be exponentially small. A standard [6] choice for this fast spatial region is

$$I_f = \left\{ \xi \in \mathbb{R} \;\middle|\; |\xi| < \frac{1}{\sqrt{\varepsilon}} \right\} \tag{2.17}$$

Indeed, $x \ll 1$ and $\xi \gg 1$ on ∂I_f. For a sketch of the orbit, see Figure 2.5.

Now, we define the *take-off* and *touchdown* sets $T_{o,d} \subset \mathcal{M}_\varepsilon$ to be the collection of base points of all Fenichel fibres in $\mathcal{W}^{\mathrm{u}}(\mathcal{M}_\varepsilon)$ resp. $\mathcal{W}^{\mathrm{s}}(\mathcal{M}_\varepsilon)$ that have points in the transverse intersection $\mathcal{W}^{\mathrm{s}}(\mathcal{M}_\varepsilon) \cap \mathcal{W}^{\mathrm{u}}(\mathcal{M}_\varepsilon)$. Detailed information on $T_{o,d}$ can be obtained by studying the fast system (2.10) on $\mathcal{M}_\varepsilon$. First, we observe that $p_\xi = O(\varepsilon^3)$ on $\mathcal{M}_\varepsilon$ so the p-coordinate on $\mathcal{M}_\varepsilon$ remains constant to leading order during the fast excursion through the V-field. Therefore, the change in the p-coordinate of the pulse is completely determined by its accumulated change during its excursion through the

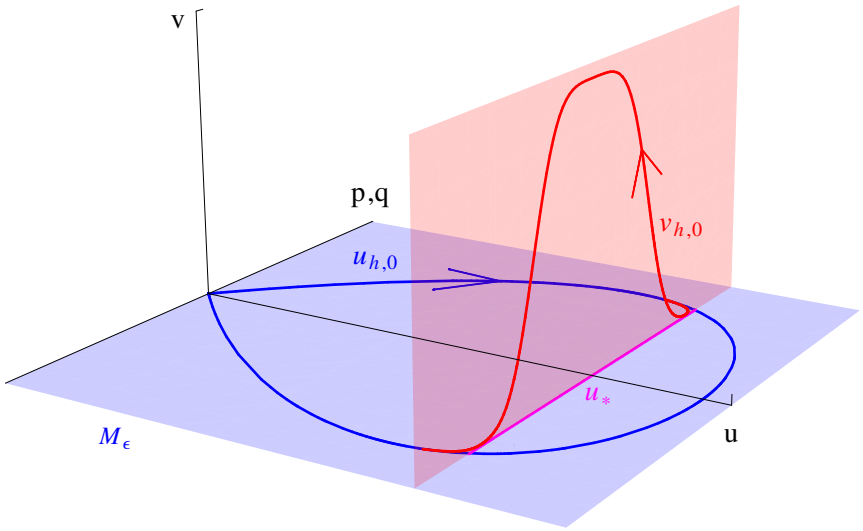

Figure 2.5: An asymptotic construction of the orbit $\gamma_h(\xi)$ of Theorem 2.2 drawn in three dimensions. The p- and q-directions are combined, since there is no direct interaction between them. The blue surface represents the persistent slow manifold $\mathcal{M}_\varepsilon$ while the fast dynamics take place on the red surface, which is spanned by the v and q directions. The slow homoclinic orbit $u_{h,0}(\chi)$ is drawn in blue, the fast homoclinic orbit $v_{h,0}(\xi; u_*, 0)$ is drawn in red. The jump through the fast field projected on $\mathcal{M}_\varepsilon$ is indicated by the purple line.

fast field, and is given by

$$\begin{aligned}\Delta_\xi p &= \int_{I_f} p_\xi \,\mathrm{d}\xi = \int_{I_f} -\varepsilon\sigma v^2 + O(\varepsilon^3)\,\mathrm{d}\xi = \int_{-\infty}^{\infty} -\varepsilon\sigma\, v_{h,0}(\xi; u_0, p_0)^2\,\mathrm{d}\xi + O(\varepsilon^2)\\ &= -6\,\varepsilon\sigma\, u_0^2 + O(\varepsilon^2)\end{aligned} \tag{2.18}$$

where we have used (2.10) and (2.13). Moreover, since $u_\xi = \varepsilon\, p$ and $p = O(\varepsilon)$ on I_f, we see that $\Delta_\xi u = O(\varepsilon^2)$. This means that during the jump through the fast field, the u-coordinate of the pulse does not change to leading order.
Since $\mathcal{W}^{\mathrm{s}}(\mathcal{M}_\varepsilon) \cap \mathcal{W}^{\mathrm{u}}(\mathcal{M}_\varepsilon)$ intersects the hyperplane $\{(u, p, v, q) \,|\, p = q = 0\}$ transversally, we can define the take-off and touchdown sets as curves

$$T_o = \left\{(u, p, 0, 0) \in \mathcal{M}_\varepsilon \,\middle|\, p = 3\,\varepsilon\,\sigma u^2\right\},\ T_d = \left\{(u, p, 0, 0) \in \mathcal{M}_\varepsilon \,\middle|\, p = -3\,\varepsilon\,\sigma u^2\right\} \tag{2.19}$$

at leading order. Note that if σ changes sign, the take-off and touchdown curves are

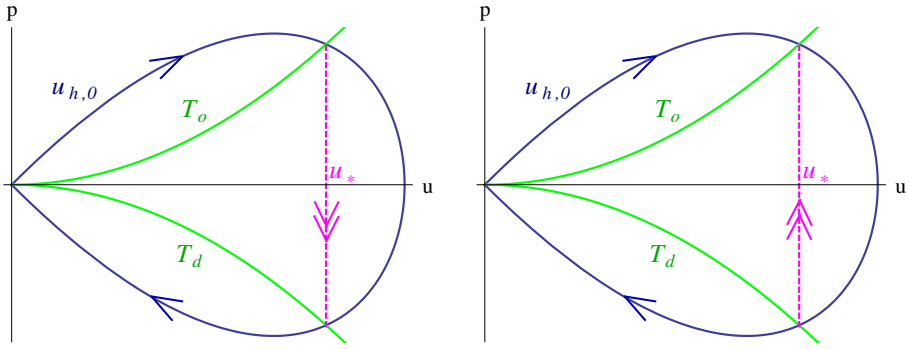

(a) For $\sigma > 0$ the jump is downwards, the resulting pulse is shown in Figure 2.1a.

(b) For $\sigma < 0$ the jump is upwards, the resulting pulse is shown in Figure 2.1b.

Figure 2.6: The homoclinic orbit $u_{h,0}(\chi)$ is drawn in blue in the (u, p)-plane. The take-off and touchdown curves $T_o = \{(u, p) \mid p = 3\,\varepsilon\,\sigma u^2\}$ and $T_d = \{(u, p) \mid p = -3\,\varepsilon\,\sigma u^2\}$ are drawn in green. The jump through the fast field at $u = u_*$ is indicated by the dashed purple line.

interchanged: for $\sigma > 0$ the take-off curve has positive p-values, while for $\sigma < 0$ the take-off curve has negative p-values. This also means the *direction* of the fast jump is reversed when σ changes sign, see (2.18) and Figure 2.6a.

An orbit of the system (2.9) / (2.10) is homoclinic to $(0, 0, 0, 0)$ if its Fenichel fibre basepoints in $T_{o,d}$ intersect the super-slow homoclinic orbit $u_{h,0} \in \mathcal{M}_\varepsilon$, see Figure 2.6a. This intersection can be determined by integrating (2.14) once,

$$\tfrac{1}{2}p^2 = \varepsilon^2\left(\tfrac{1}{2}\alpha\,u^2 - \frac{\gamma}{d+1}\,u^{d+1}\right) \tag{2.20}$$

and substituting $p = \pm 3\,\varepsilon\,\sigma u^2$ from (2.19) to obtain

$$\frac{2\gamma}{d+1}u^{d-1} = \alpha - 9\,\sigma^2 u^2 \tag{2.21}$$

which for $\alpha, \gamma, |\sigma| > 0$ and $d > 1$ always has a unique real positive solution, denoted by u_*. Furthermore, we define χ_* as the (unique) *positive* χ-value for which $u_{h,0}(\chi_*) = u_*$, the u-coordinate of the intersection. When $\sigma < 0$, we obtain a slightly different pulse since part of the slow homoclinic orbit $u_{h,0}$ is covered twice, see Figure 2.6b. This has its consequences for the formulation of our main existence result:

Theorem 2.2. *Let $\varepsilon > 0$ be sufficiently small. Then, for all values of the parameters $\alpha > 0$, $\gamma > 0$, $|\sigma| > 0$ and $d > 1$, there exists a unique orbit $\gamma_h(\xi) = (u_h(\xi), p_h(\xi), v_h(\xi), q_h(\xi))$ as a solution of system* (2.10) *which is homoclinic to* $(0,0,0,0)$ *and lies in the intersection $\mathcal{W}^{\mathrm{s}}(\mathcal{M}_\varepsilon) \cap \mathcal{W}^{\mathrm{u}}(\mathcal{M}_\varepsilon)$. Moreover,*

$$\begin{aligned} \|v_h(\xi) - v_{h,0}(\xi; u_*, 0)\|_\infty &= O(\varepsilon)\,, \\ \|q_h(\xi) - \tfrac{\mathrm{d}}{\mathrm{d}\xi} v_{h,0}(\xi; u_*, 0)\|_\infty &= O(\varepsilon) \end{aligned} \tag{2.22}$$

for all $\xi \in \mathbb{R}$ and

$$\begin{aligned} \|u_h(\chi) - u_{h,0}(\chi - \operatorname{sgn}(\sigma)\chi_*)\|_\infty &= O(\varepsilon)\,, \\ \|p_h(\chi) - \varepsilon \tfrac{\mathrm{d}}{\mathrm{d}\chi} u_{h,0}(\chi - \operatorname{sgn}(\sigma)\chi_*)\|_\infty &= O(\varepsilon) \end{aligned} \tag{2.23}$$

for all $\chi < 0$, while

$$\begin{aligned} \|u_h(\chi) - u_{h,0}(\chi + \operatorname{sgn}(\sigma)\chi_*)\|_\infty &= O(\varepsilon)\,, \\ \|p_h(\chi) - \varepsilon \tfrac{\mathrm{d}}{\mathrm{d}\chi} u_{h,0}(\chi + \operatorname{sgn}(\sigma)\chi_*)\|_\infty &= O(\varepsilon) \end{aligned} \tag{2.24}$$

for all $\chi > 0$.

The orbit γ_h corresponds to a homoclinic pulse solution (U_h, V_h) of system (2.7)*.*

Proof. The missing details in the above geometric construction, especially in the precise estimates of (2.22), (2.23) and (2.24), can be obtained in a manner identical to the corresponding result on 'slowly linear' systems in [6]. □

2.3 Pulse stability: analysis

The linear stability of the stationary pulse solution (U_h, V_h) of (2.7) found in the previous section is determined by adding a perturbation of the form $(\bar{u}(x), \bar{v}(x))\, e^{\lambda t}$ and linearising equation (2.7) around the stationary solution, obtaining in the fast variable ξ,

$$\begin{cases} \bar{u}_\xi = \varepsilon\, \bar{p} & \text{(2.25a)} \\ \bar{p}_\xi = -2\,\varepsilon\,\sigma\, V_h(\xi)\, \bar{v} + \varepsilon^3 \left(\alpha + \lambda - \gamma\, d\, U_h(\xi)^{d-1}\right) \bar{u} & \text{(2.25b)} \\ \bar{v}_\xi = \bar{q} & \text{(2.25c)} \\ \bar{q}_\xi = \left(1 + \lambda - 2\dfrac{V_h(\xi)}{U_h(\xi)}\right) \bar{v} + \dfrac{V_h(\xi)^2}{U_h(\xi)^2}\, \bar{u} & \text{(2.25d)} \end{cases}$$

We write the fast system (2.25) in vector form

$$\frac{\mathrm{d}}{\mathrm{d}\xi}\phi = A(\xi;\lambda,\varepsilon)\phi \tag{2.26}$$

where $\phi(\xi) = ((\bar{u}(\xi), \bar{p}(\xi), \bar{v}(\xi), \bar{q}(\xi))^T$ and

$$A(\xi;\lambda,\varepsilon) = \begin{pmatrix} 0 & \varepsilon & 0 & 0 \\ \varepsilon^3\left(\alpha+\lambda-\gamma\, d\, U_h(\xi)^{d-1}\right) & 0 & 2\,\varepsilon\,\sigma\, V_h(\xi) & 0 \\ 0 & 0 & 0 & 1 \\ \frac{V_h(\xi)^2}{U_h(\xi)^2} & 0 & 1+\lambda-2\frac{V_h(\xi)}{U_h(\xi)} & 0 \end{pmatrix} \tag{2.27}$$

Since the V-component of the stationary pulse decays much faster than its U-component, the ratio $\frac{V_h}{U_h}$ is well-defined and converges to zero as $\xi \to \pm\infty$. This results in the constant coefficient matrix

$$A_\infty(\lambda,\varepsilon) = \lim_{|\xi|\to\infty} A(\xi;\lambda,\varepsilon) = \begin{pmatrix} 0 & \varepsilon & 0 & 0 \\ \varepsilon^3(\alpha+\lambda) & 0 & 0 & 0 \\ 0 & 0 & 0 & 1 \\ 0 & 0 & 1+\lambda & 0 \end{pmatrix} \tag{2.28}$$

which has eigenvalues

$$\pm\,\Lambda_f = \pm\sqrt{1+\lambda} \quad \text{and} \quad \pm\,\varepsilon^2\Lambda_s = \pm\varepsilon^2\sqrt{\alpha+\lambda} \tag{2.29}$$

and associated eigenvectors

$$E_{f,\pm} = \left(0,0,1,\pm\sqrt{1+\lambda}\right)^T \quad \text{and} \quad E_{s,\pm} = \left(1,\pm\varepsilon\sqrt{\alpha+\lambda},0,0\right)^T. \tag{2.30}$$

The essential spectrum of the linear eigenvalue problem (2.25) therefore is

$$\sigma_{\mathrm{ess}} = \{\lambda\in\mathbb{R}\,|\,\lambda \le \max(-\alpha,-1)\}, \tag{2.31}$$

see [45]. Since $\alpha > 0$, we can conclude that the stability of the pulse (U_h, V_h) is determined by its discrete spectrum.

2.3.1 The Evans function and its decomposition

The Evans function, which is complex analytic outside the essential spectrum – see [3, 45] and the references therein – associated to system (2.25) can be defined by

$$\mathcal{D}(\lambda,\varepsilon) = \det\left[\phi_i(\xi;\lambda,\varepsilon)\right] \tag{2.32}$$

where the functions ϕ_i, $i = 1,2,3,4$ satisfy boundary conditions at $\pm\infty$ (see below) and span the solution space of (2.25). The eigenvalues of (2.26) outside σ_{ess} coincide with the roots of $\mathcal{D}(\lambda,\varepsilon)$, including multiplicities.

Definition 2.3. *A statement of the form '$f(x) \rightsquigarrow c\, g(x)$ as $x \to \infty$' is true whenever the limit* $\lim_{x\to\infty} \frac{1}{g(x)} f(x) = c$ *exists and is well-defined.*

Lemma 2.4. *For all $\lambda \in \mathbb{C} \setminus \sigma_{\text{ess}}$, there are solutions $\phi_{f,\text{L/R}}(\xi;\lambda,\varepsilon)$ and $\phi_{s,\text{L/R}}(\xi;\lambda,\varepsilon)$ to* (2.25) *such that the set $\left\{\phi_{f,\text{L/R}}(\xi;\lambda,\varepsilon), \phi_{s,\text{L/R}}(\xi;\lambda,\varepsilon)\right\}$ spans the solution space of* (2.25) *and*

$$\phi_{f,\text{L}}(\xi;\lambda,\varepsilon) \rightsquigarrow E_{f,+}\, e^{\Lambda_f \xi} \quad as \quad \xi \to -\infty \tag{2.33a}$$
$$\phi_{f,\text{R}}(\xi;\lambda,\varepsilon) \rightsquigarrow E_{f,-}\, e^{-\Lambda_f \xi} \quad as \quad \xi \to \infty \tag{2.33b}$$
$$\phi_{s,\text{L}}(\xi;\lambda,\varepsilon) \rightsquigarrow E_{s,+}\, e^{\varepsilon^2 \Lambda_s \xi} \quad as \quad \xi \to -\infty \tag{2.33c}$$
$$\phi_{s,\text{R}}(\xi;\lambda,\varepsilon) \rightsquigarrow E_{s,-}\, e^{-\varepsilon^2 \Lambda_s \xi} \quad as \quad \xi \to \infty \tag{2.33d}$$

Moreover, there exist analytic transmission functions $t_{f,+}(\lambda,\varepsilon)$ and $t_{s,+}(\lambda,\varepsilon)$ such that

$$\phi_{f,\text{L}}(\xi;\lambda,\varepsilon) \rightsquigarrow t_{f,+}(\lambda,\varepsilon)\, E_{f,+}\, e^{\Lambda_f \xi} \quad as \quad \xi \to \infty \tag{2.34a}$$
$$\phi_{s,\text{L}}(\xi;\lambda,\varepsilon) \rightsquigarrow t_{s,+}(\lambda,\varepsilon)\, E_{s,+}\, e^{\varepsilon^2 \Lambda_s \xi} \quad as \quad \xi \to \infty \tag{2.34b}$$

where $t_{s,+}(\lambda,\varepsilon)$ is only defined if $t_{f,+}(\lambda,\varepsilon) \neq 0$. These choices, when possible, determine $\phi_{f,\text{L/R}}$ and $\phi_{s,\text{L}}$ uniquely.

Proof. Although the linearised system 2.26 is not identical to its counterpart in [6], exactly the same arguments as in [6] can be applied here. Therefore, we refer to [6] for the details of the proof. □

The Evans function can be determined by taking the limit $\xi \to \infty$ of the determinant of the functions defined in Lemma 2.4, since the Evans function itself does not depend on ξ since the trace of $A(\xi;\lambda,\varepsilon)$ vanishes (Abel's theorem). This yields (see [6])

$$\mathcal{D}(\lambda,\varepsilon) = 4\varepsilon\, t_{f,+}(\lambda,\varepsilon)\, t_{s,+}(\lambda,\varepsilon)\, \sqrt{1+\lambda}\, \sqrt{\alpha+\lambda} \tag{2.35}$$

Corollary 2.5. *The set of eigenvalues of* (2.26) *is contained in the union of the sets of roots of $t_{f,+}(\lambda,\varepsilon)$ and $t_{s,+}(\lambda,\varepsilon)$.*

Note that, due to the fact that $t_{s,+}(\lambda,\varepsilon)$ only defined when $t_{f,+}(\lambda,\varepsilon) \neq 0$, the Evans function $\mathcal{D}(\lambda,\varepsilon)$ does not necessarily vanish when $t_{f,+}(\lambda,\varepsilon) = 0$. This is called the 'resolution to the NLEP paradox' in [6, 7]. The roots of $t_{f,+}$ will be discussed later, in section 2.3.3.

2.3.2 The slow solution $\phi_{s,\mathrm{L}}$ outside I_f

To obtain more information about the roots of $t_{s,+}(\lambda,\varepsilon)$, it is necessary to determine the leading order behaviour of $\phi_{s,\mathrm{L}}(\xi;\lambda,\varepsilon)$ in the different coordinate regimes. From Lemma 2.4 we know that $\phi_{s,\mathrm{L}}$ is *slowly growing* in ξ, since its leading order behaviour for both $\xi \to \pm\infty$ is determined by the exponential growth factor $\varepsilon^2\Lambda_s = O(\varepsilon^2)$. However, the dynamics governing $\phi_{s,\mathrm{L}}$ differ significantly inside and outside the fast spatial region I_f. Based on our knowledge of the homoclinic solution stated in Theorem 2.2, we can infer the form of the matrix $A(\xi;\lambda,\varepsilon)$ both inside and outside I_f:

$$A_f(\xi;\lambda,\varepsilon) = \begin{pmatrix} 0 & \varepsilon & 0 & 0 \\ \varepsilon^3\left(\alpha+\lambda-\gamma\, d\, u_*^{d-1}\right) & 0 & 2\,\varepsilon\,\sigma\, v_{h,0}(\xi;u_*,0) & 0 \\ 0 & 0 & 0 & 1 \\ \frac{v_{h,0}(\xi;u_*,0)^2}{u_*^2} & 0 & 1+\lambda-2\frac{v_{h,0}(\xi;u_*,0)}{u_*} & 0 \end{pmatrix} \tag{2.36}$$

to leading order for $\xi \in I_f$ and

$$A_s(\xi;\lambda,\varepsilon) = \begin{pmatrix} 0 & \varepsilon & 0 & 0 \\ \varepsilon^3\left(\alpha+\lambda-\gamma\, d\, u_{h,0}(|\varepsilon^2\xi|+\mathrm{sgn}(\sigma)\chi_*)^{d-1}\right) & 0 & 0 & 0 \\ 0 & 0 & 0 & 1 \\ 0 & 0 & 1+\lambda & 0 \end{pmatrix} \tag{2.37}$$

for $\xi \notin I_f$ to leading order.
Note that it is the fact that this 'intermediate' slow matrix exists, or better: that it is not identical to $A_\infty(\lambda,\varepsilon)$ (2.28), that distinguishes the 'slowly nonlinear Gierer-Meinhardt problem' from 'slowly linear' problems as the classical Gierer-Meinhardt or Gray-Scott systems. Note also that a intermediate matrix as $A_s(\xi;\lambda,\varepsilon)$ was already encountered in [8], in the study of a system with non-exponential (algebraic) decay.

Lemma 2.6. *Consider the system*

$$\tfrac{\mathrm{d}}{\mathrm{d}\xi}\psi = A_s(\xi;\lambda,\varepsilon)\psi \tag{2.38}$$

with $A_s(\xi;\lambda,\varepsilon)$ as given in (2.37)*. There exist solutions $\psi_{f,\pm}(\xi;\lambda,\varepsilon)$ and $\psi_{s,\pm}(\xi;\lambda,\varepsilon)$ which span the solution space of* (2.38) *for $\xi < -\frac{1}{\sqrt{\varepsilon}}$ and*

$$\psi_{f,+}(\xi;\lambda,\varepsilon) \rightsquigarrow E_{f,+}\, e^{\Lambda_f\xi}, \quad \psi_{s,+}(\xi;\lambda,\varepsilon) \rightsquigarrow E_{s,+}\, e^{\varepsilon^2\Lambda_s\xi}, \tag{2.39a}$$

$$\psi_{f,-}(\xi;\lambda,\varepsilon) \rightsquigarrow E_{f,-}\, e^{-\Lambda_f\xi}, \quad \psi_{s,-}(\xi;\lambda,\varepsilon) \rightsquigarrow E_{s,-}\, e^{-\varepsilon^2\Lambda_s\xi} \tag{2.39b}$$

as $\xi \to -\infty$.

Proof. The same arguments as in the proof of Lemma 2.4 can be used, because $\lim_{\xi\to-\infty} A_s(\xi;\lambda,\varepsilon) = A_\infty(\lambda,\varepsilon)$. □

Since $A(\xi;\lambda,\varepsilon)$ is to leading order equal to $A_s(\xi;\lambda,\varepsilon)$ for $\xi < -\frac{1}{\sqrt{\varepsilon}}$ and both $\phi_{s,\mathrm{L}}$ and $\psi_{s,+} \rightsquigarrow E_{s,+}\, e^{\varepsilon^2\Lambda_s\xi}$ as $\xi \to -\infty$, combining Lemma 2.4 and Lemma 2.6 yields the following Corollary:

Corollary 2.7. *For $\xi < -\frac{1}{\sqrt{\varepsilon}}$, we can write*

$$\phi_{s,\mathrm{L}}(\xi;\lambda,\varepsilon) = \psi_{s,+}(\xi;\lambda,\varepsilon)$$

to leading order.

The slow evolution of the $\bar{u}$-component of $\psi_{s,\pm}$ can be written, again using $\chi = \varepsilon^2\xi$, as

$$\bar{u}_{\chi\chi} - \left(\alpha + \lambda - \gamma\, d\, u_h(|\chi| + \mathrm{sgn}(\sigma)\chi_*)^{d-1}\right)\bar{u} = 0 \tag{2.40}$$

We can introduce the coordinate transformation

$$\begin{aligned} z &= -\frac{1}{\sqrt{\alpha}}\frac{\frac{\mathrm{d}}{\mathrm{d}\chi}u_{h,0}(\chi - \mathrm{sgn}(\sigma)\chi_*)}{u_{h,0}(\chi - \mathrm{sgn}(\sigma)\chi_*)} \\ &= \frac{1}{\sqrt{\alpha}}\frac{\mathrm{d}}{\mathrm{d}\chi}\log\frac{1}{u_{h,0}(\chi - \mathrm{sgn}(\sigma)\chi_*)} \\ &= \tanh\left(\tfrac{1}{2}(d-1)\sqrt{\alpha}\,(\chi - \mathrm{sgn}(\sigma)\chi_*)\right) \end{aligned} \tag{2.41}$$

(by (2.16)) for the region $\chi < 0$ to obtain

$$(1-z^2)\,\bar{u}_{zz} - 2\,z\,\bar{u}_z + \left(\nu(\nu+1) - \frac{\mu^2}{1-z^2}\right)\bar{u} = 0 \tag{2.42}$$

where

$$\nu = \frac{d+1}{d-1} \tag{2.43a}$$

$$\mu = +\frac{2}{d-1}\sqrt{1+\frac{\lambda}{\alpha}} \tag{2.43b}$$

where we have chosen the branch cut associated to σ_{ess} such that $\mathrm{Re}\,\mu > 0$; note that $\nu > 1$. Equation (2.42) is the Legendre differential equation: its solutions are the associated Legendre functions $P^\mu_\nu(z)$ and $Q^\mu_\nu(z)$ [1, 2]. Given the symmetry $z \to -z$ of the equation, we choose the basis of the solution space to be $P^\mu_\nu(\pm z)$. The limit

$\chi \to -\infty$ corresponds to the limit $z \to -1$. Taking into account the normalisation of $\psi_{s,+}$ from Lemma 2.6, the correct expression for the $\bar{u}$-component of $\psi_{s,+}$ is

$$\bar{u}(\chi) = \Gamma(1+\mu)\, e^{\Lambda_s \mathrm{sgn}(\sigma)\chi_*} P_\nu^{-\mu}(-z(\chi)) \tag{2.44}$$

such that

$$\lim_{\chi \uparrow 0} \bar{u}(\chi) = \Gamma(1+\mu)\, e^{\Lambda_s \mathrm{sgn}(\sigma)\chi_*} P_\nu^{-\mu}(z_*) \tag{2.45}$$

where we define

$$z_* = \mathrm{sgn}(\sigma)\, \tanh\left(\tfrac{1}{2}(d-1)\sqrt{\alpha}\chi_*\right) \tag{2.46}$$

We can express z_* in terms of u_* using equation (2.15): integrating once yields

$$u_\chi^2 = \alpha\, u^2 - \frac{2\gamma}{d+1} u^{d+1} \tag{2.47}$$

so, by equation (2.41)

$$z^2 = \frac{1}{\alpha}\frac{u_\chi^2}{u^2} = 1 - \frac{2\gamma}{\alpha(d+1)} u^{d-1} \tag{2.48}$$

hence

$$\alpha\left(1 - z_*^2\right) = \frac{2\gamma}{d+1} u_*^{d-1} = \alpha - 9\sigma^2 u_*^2 \tag{2.49}$$

by equation (2.21); from this, we conclude that

$$z_* = \frac{3\,\sigma}{\sqrt{\alpha}}\, u_*. \tag{2.50}$$

Note that z_* inherits the sign of σ since χ_* is chosen to be positive, see section 2.2.1.

Lemma 2.8. *Let $\bar{u}_s(\xi;\lambda,\varepsilon)$ be the $\bar{u}$-component of $\phi_{s,\mathrm{L}}(\xi;\lambda,\varepsilon)$ as defined in Lemma 2.4. Then*

$$\bar{u}_s(\xi) = \Gamma(1+\mu)\, e^{\Lambda_s \mathrm{sgn}(\sigma)\chi_*} P_\nu^{-\mu}(z_*) + O(\varepsilon\sqrt{\varepsilon}) \quad \textit{for} \quad \xi \in I_f. \tag{2.51}$$

Moreover, there are two transmission functions $t_{s,+}(\lambda,\varepsilon)$ and $t_{s,-}(\lambda,\varepsilon)$ such that

$$\phi_{s,\mathrm{L}}(\xi;\lambda,\varepsilon) = t_{s,+}(\lambda,\varepsilon)\,\psi_{s,-}(-\xi;\lambda,\varepsilon) + t_{s,-}(\lambda,\varepsilon)\,\psi_{s,+}(-\xi;\lambda,\varepsilon) \quad \textit{for} \quad \xi > \frac{1}{\sqrt{\varepsilon}} \tag{2.52}$$

up to exponentially small terms in ξ, where $t_{s,+}$ was already introduced in Lemma 2.4.

Proof. The $\bar{u}$-component of $\phi_{s,\mathrm{L}}$ is constant on I_f, since both $\frac{\mathrm{d}}{\mathrm{d}\xi}\bar{u}_s$ and $\frac{\mathrm{d}}{\mathrm{d}\xi}\bar{p}_{s,+}$ are asymptotically small on I_f. Therefore, we can determine its leading order value using Corollary 2.7 and (2.45). The matrix A_s as defined in (2.37) is symmetric in ξ. For the region $\xi > \frac{1}{\sqrt{\varepsilon}}$ we can therefore use the same $\psi_{f,\pm}$ and $\psi_{s,\pm}$ from Lemma 2.6 as a basis for the solution space in this region, under the reflection $\xi \to -\xi$. The role of $\psi_{s,+}$ and $\psi_{s,-}$ is reversed compared to the interval $\xi < -\frac{1}{\sqrt{\varepsilon}}$: we see that $\psi_{s,-}(-\xi)$ grows (slowly) exponentially as $\xi \to \infty$, whereas $\psi_{s,+}(-\xi)$ has an exponential (slow) decay under the same limit. The normalisation of $\phi_{s,\mathrm{L}}$ for $\xi \to \infty$, which by Lemma 2.4 introduces $t_{s,+}(\lambda,\varepsilon)$ in (2.52), does not exclude the possibility that for $\xi > \frac{1}{\sqrt{\varepsilon}}$, $\phi_{s,\mathrm{L}}$ has components which *decay* (slowly) as $\xi \to \infty$. Therefore, we write the leading order expression of $\phi_{s,\mathrm{L}}$ in this region as a linear combination of a slowly increasing and a slowly decreasing component, and introduce $t_{s,-}(\lambda,\varepsilon)$ to measure the decreasing component. A term containing the fast decreasing component is omitted, since for $\xi > \frac{1}{\sqrt{\varepsilon}}$ this would only give an exponentially small correction to the result in (2.52). □

Based on the results of Lemma 2.8, we have

$$\lim_{\chi \downarrow 0} \bar{u}_s(\chi) = \Gamma(1+\mu)\left[t_{s,+}(\lambda,\varepsilon)\, P_\nu^{-\mu}(-z_*) + t_{s,-}(\lambda,\varepsilon)\, P_\nu^{-\mu}(z_*)\right] \tag{2.53}$$

to leading order.

Corollary 2.9. *Combining equations* (2.51) *and* (2.53) *yields*

$$t_{s,+}(\lambda,\varepsilon)\, P_\nu^{-\mu}(-z_*) + t_{s,-}(\lambda,\varepsilon)\, P_\nu^{-\mu}(z_*) = P_\nu^{-\mu}(z_*) + O(\varepsilon\sqrt{\varepsilon}) \tag{2.54}$$

to leading order.

This gives a (first) relation between $t_{s,+}(\lambda,\varepsilon)$ and $t_{s,-}(\lambda,\varepsilon)$.

2.3.3 The fast components of $\phi_{s,\mathrm{L}}$ inside I_f

Since $\bar{u}_s(\xi;\lambda,\varepsilon)$ is constant to leading order for $\xi \in I_f$ (see Lemma 2.8), we can represent it by its value at $0 \in I_f$. Moreover, the equation for the $\bar{v}$-component in (2.25) decouples and yields an inhomogeneous Sturm-Liouville problem,

$$\bar{v}_{\xi\xi} - \left((1+\lambda) - \frac{2}{u_*}\, v_{h,0}(\xi;u_*,0)\right)\bar{v} = \frac{1}{u_*^2}\, v_{h,0}(\xi;u_*,0)^2\, \bar{u}_s(0) \tag{2.55}$$

where we used that $u_h(\xi) = u_*$ and $v_h(\xi) = v_{h,0}(\xi;u_*,0)$ for $\xi \in I_f$ to leading order (see Theorem 2.2). Based on the slow behaviour of $\phi_{s,\mathrm{L}}$ determined in Lemmas 2.4

and 2.8, we observe that the solution $\bar{v}$ of (2.55) must extinguish as $\xi \to \partial I_f$, which implies that $\bar{v}$ must decay exponentially fast in ξ.

By the nature of the Gierer-Meinhardt equation (2.4) and its 'slow nonlinearity' the problem can be solved exactly along the same lines as done in section 2.3.2 for the slow problem. First, we introduce a coordinate transformation similar to (2.41),

$$\zeta = -\frac{\frac{\mathrm{d}}{\mathrm{d}\xi} v_{h,0}(\xi; u_*, 0)}{v_{h,0}(\xi; u_*, 0)} = \frac{\mathrm{d}}{\mathrm{d}\xi} \log \frac{1}{v_{h,0}(\xi; u_*, 0)} = \tanh\left(\tfrac{1}{2}\xi\right) \tag{2.56}$$

using (2.13). In this coordinate, v_h can be written as

$$v_h(\zeta; u_*, 0) = \frac{3\,u_*}{2}\left(1 - \zeta^2\right) \tag{2.57}$$

and equation (2.55) is transformed to

$$(1-\zeta^2)\,\bar{v}_{\zeta\zeta} - 2\,\zeta\,\bar{v}_\zeta + \left(12 - \frac{4(1+\lambda)}{1-\zeta^2}\right)\bar{v} = 9\,\bar{u}_s(0)\,(1-\zeta^2) \tag{2.58}$$

and $I_f = \{\zeta \in \mathbb{R} \mid |\zeta| < 1\}$ up to exponentially small terms, compare (2.17).
Its homogeneous reduction

$$(1-\zeta^2)\,\bar{v}_{\zeta\zeta} - 2\,\zeta\,\bar{v}_\zeta + \left(12 - \frac{4(1+\lambda)}{1-\zeta^2}\right)\bar{v} = 0 \tag{2.59}$$

can again be solved using associated Legendre functions; it is a special case ($\alpha = 1$, $d = 2$) of the slow eigenvalue problem (2.42).

It should be noted that there is a crucial difference between (2.42) and (2.58). The slow equation (2.42) is only defined on part of the 'full' domain: $z \in (-1, z_*) \subset (-1, 1)$. Therefore, the eigenvalues of (2.42) do not yield direct implications for the stability of the pulse (U_h, V_h). This is very different from the fast system (2.58). It has three eigenvalues; its corresponding eigenfunctions are

$$\lambda_f^{(0)} = \frac{5}{4}, \quad \bar{v}_f^{(0)}(\zeta) = \left(1-\zeta^2\right)^{\frac{3}{2}} \tag{2.60a}$$

$$\lambda_f^{(1)} = 0, \quad \bar{v}_f^{(1)}(\zeta) = \zeta\left(1-\zeta^2\right) = -\frac{2}{3u_*}\frac{\mathrm{d}\zeta}{\mathrm{d}\xi}\frac{\mathrm{d}}{\mathrm{d}\zeta} v_h(\zeta; u_*, 0) \tag{2.60b}$$

$$\lambda_f^{(2)} = -\frac{3}{4}, \quad \bar{v}_f^{(2)}(\zeta) = \left(\zeta^2 - \tfrac{1}{5}\right)\sqrt{1-\zeta^2} \tag{2.60c}$$

Referring to [6], we recall that the roots of $t_{f,+}(\lambda, \varepsilon)$ are to leading order given by the eigenvalues of (2.59), so we have the following Lemma:

Lemma 2.10. *There are unique* $\lambda^{(i)}(\varepsilon) \in \mathbb{R}$ *such that* $\lim_{\varepsilon\to 0} \lambda^{(i)}(\varepsilon) = \lambda_f^{(i)}$ *and* $t_{f,+}(\lambda^{(i)}(\varepsilon), \varepsilon) = 0$ *with multiplicity 1 for* $i = 0, 1, 2$.

Proof. See [6]. □

Hence, the eigenvalues of (2.59) are to leading order zeroes of the fast component of the Evans function $\mathcal{D}(\lambda, \varepsilon)$ given in (2.35) and thus in principle candidates for being zeroes of the full Evans function.

For all $\lambda \in \mathbb{C} \setminus \sigma_{\text{ess}}$, the solution space of (2.59) is spanned by the associated Legendre functions

$$\bar{v}_\pm(\zeta; \lambda) = c_\pm(\lambda) P_3^{-2\sqrt{1+\lambda}}(\pm\zeta); \qquad \lim_{\zeta\to\pm 1} \bar{v}_\pm(\zeta; \lambda) = 0 \tag{2.61}$$

where we normalise $\bar{v}_\pm$ (i.e. choose $c_\pm$) such that their Wronskian is given by

$$W(\bar{v}_-, \bar{v}_+)(\zeta; \lambda) = \frac{1}{1-\zeta^2} \tag{2.62}$$

which implies that

$$c_+(\lambda)\, c_-(\lambda) = -\frac{1}{2}\, \Gamma\left(4 + 2\sqrt{1+\lambda}\right) \Gamma\left(-3 + 2\sqrt{1+\lambda}\right) \tag{2.63}$$

Indeed, the expression in (2.63) has poles at $\lambda = \lambda_f^{(i)}$, $i = 0, 1, 2$. This is due to the fact that $\bar{v}_\pm(\zeta; \lambda)$ cannot span the two-dimensional solution space for $\lambda = \lambda_f^{(i)}$. Since we have normalised the Wronskian (2.62), this is now encoded in the values of $c_\pm(\lambda)$.

We know that the inhomogeneous equation (2.58) has a unique bounded solution $\bar{v}_{\text{in}}(\xi; \lambda)$ for all $\lambda \in \mathbb{C} \setminus \sigma_{\text{ess}}$ and $\lambda \neq \lambda_f^{(0,1,2)}$. It can be determined using the Green's function

$$G(\zeta, s; \lambda) = \begin{cases} \dfrac{\bar{v}_-(s; \lambda)\, \bar{v}_+(\zeta; \lambda)}{W(\bar{v}_-, \bar{v}_+)(s; \lambda)\,(1-s^2)} & s < \zeta \\ \dfrac{\bar{v}_-(\zeta; \lambda)\, \bar{v}_+(s; \lambda)}{W(\bar{v}_-, \bar{v}_+)(s; \lambda)\,(1-s^2)} & s > \zeta \end{cases} \tag{2.64}$$

so that

$$\begin{aligned} \bar{v}_{\text{in}}(\zeta; \lambda) &= \int_{-1}^{1} 9\, \bar{u}_s(0)\, (1-s^2)\, G(\zeta, s; \lambda)\, \mathrm{d}s \\ &= 9\, \bar{u}_s(0) \left[\bar{v}_+(\zeta; \lambda) \int_{-1}^{\zeta} (1-s^2)\, \bar{v}_-(s; \lambda)\, \mathrm{d}s + \bar{v}_-(\zeta; \lambda) \int_{\zeta}^{1} (1-s^2)\, \bar{v}_+(s; \lambda)\, \mathrm{d}s \right] \end{aligned} \tag{2.65}$$

Note that the inhomogeneous term in (2.58) is only orthogonal to the eigenfunction corresponding to $\lambda_f^{(1)} = 0$; for the other two eigenvalues the solvability condition

$$\int_{-1}^{1} 9\,\bar{u}_s(0)\,(1-\zeta^2)\,\bar{v}_f^{(i)}(\zeta)\,\mathrm{d}\zeta = 0 \quad i = 0, 1, 2 \tag{2.66}$$

is not satisfied since both $\bar{v}_f^{(0,2)}(\zeta)$ and $9(1-\zeta^2)$ are even functions in ζ. This means that $\bar{v}_{\text{in}}$ as a function of λ has a simple pole at $\lambda_f^{(0)}$ and $\lambda_f^{(2)}$, and is smooth at $\lambda_f^{(1)} = 0$.

To summarise this section, the resulting expression of $\bar{v}_{\text{in}}$ is restated in the following Lemma:

Lemma 2.11. *The unique solution $\bar{v}_{in}(\zeta;\lambda)$ to equation* (2.58) *is given by*

$$\bar{v}_{\text{in}}(\zeta;\lambda) = 9\,\bar{u}_s(0)\left[\bar{v}_+(\zeta;\lambda)\int_{-1}^{\zeta}(1-s^2)\,\bar{v}_-(s;\lambda)\,\mathrm{d}s + \bar{v}_-(\zeta;\lambda)\int_{\zeta}^{1}(1-s^2)\,\bar{v}_+(s;\lambda)\,\mathrm{d}s\right] \tag{2.67}$$

with $v_\pm(\zeta;\lambda)$ as defined in (2.61) *and subject to condition* (2.63).

2.3.4 The slow transmission function $t_{s,+}(\lambda,\varepsilon)$

In section 2.3.2 we studied $\phi_{s,\text{L}}$ outside I_f and in section 2.3.3 we considered its fast dynamics inside I_f. However, we did not yet combine these results.
Using (2.25), we see that

$$\begin{aligned}\bar{u}_{\xi\xi} &= -2\,\varepsilon^2\sigma\,V_h(\xi)\,\bar{v} + O(\varepsilon^4)\\ &= -2\,\varepsilon^2\sigma\,v_{h,0}(\xi;u_*,0)\,\bar{v}_{\text{in}}\,(\zeta(\xi);\lambda)\end{aligned} \tag{2.68}$$

to leading order in I_f. Thus, the total change of $\bar{u}_\xi$ over I_f is given by

$$\begin{aligned}\Delta_\xi\bar{u}_\xi &= \int_{I_f} u_{\xi\xi}\,\mathrm{d}\xi\\ &= -2\,\varepsilon^2\sigma\int_{-\infty}^{\infty} v_{h,0}(\xi;u_*,0)\,\bar{v}_{\text{in}}\,(\zeta(\xi);\lambda)\;\mathrm{d}\xi\\ &= -2\,\varepsilon^2\sigma\int_{-1}^{1} v_{h,0}\,(\xi(\zeta);u_*,0)\;\bar{v}_{\text{in}}\,(\zeta;\lambda)\;\frac{2\,\mathrm{d}\zeta}{1-\zeta^2}\\ &= -2\,\varepsilon^2\sigma\int_{-1}^{1}\frac{3\,u_*}{2}\,(1-\zeta^2)\,\bar{v}_{\text{in}}\,(\zeta;\lambda)\;\frac{2\,\mathrm{d}\zeta}{1-\zeta^2}\\ &= -6\,\varepsilon^2\sigma\,u_*\int_{-1}^{1}\bar{v}_{\text{in}}\,(\zeta;\lambda)\;\mathrm{d}\zeta := \Delta_f\end{aligned} \tag{2.69}$$

all to leading order. Using the expression for $\bar{v}_{\text{in}}(\zeta;\lambda)$ from Lemma 2.11 and the symmetry in ζ between $\bar{v}_+$ and $\bar{v}_-$, this can be rewritten as

$$\Delta_f = -108\,\varepsilon^2\sigma\,u_*\,\bar{u}_s(0)\int_{-1}^{1}\int_{-1}^{\zeta}\bar{v}_+(\zeta;\lambda)\,\bar{v}_-(s;\lambda)(1-s^2)\,\mathrm{d}s\,\mathrm{d}\zeta \tag{2.70}$$

The desired coupling between the slow and fast dynamics can now be obtained by realising that this change in $\bar{u}_\xi$ should match with the slow behaviour of $\phi_{s,\mathrm{L}}$ outside I_f. Using Corollary 2.7 and Lemma 2.8,

$$\begin{aligned}\Delta_f = \Delta_\xi\bar{u}_\xi &= \bar{u}_\xi\left(\tfrac{1}{\sqrt{\varepsilon}}\right) - \bar{u}_\xi\left(-\tfrac{1}{\sqrt{\varepsilon}}\right)\\ &= \varepsilon^2\,\Gamma(1+\mu)\frac{\mathrm{d}z}{\mathrm{d}\chi}\frac{\mathrm{d}}{\mathrm{d}z}\left[t_{s,+}\,P_\nu^{-\mu}(-z) + t_{s,-}\,P_\nu^{-\mu}(z)\right]_{z=z_*}\\ &\quad - \varepsilon^2\Gamma(1+\mu)\frac{\mathrm{d}z}{\mathrm{d}\chi}\frac{\mathrm{d}}{\mathrm{d}z}\left[P_\nu^{-\mu}(-z)\right]_{z=-z_*}\\ &= \varepsilon^2\,\Gamma(1+\mu)\frac{\mathrm{d}z}{\mathrm{d}\chi}\frac{\mathrm{d}}{\mathrm{d}z}\left[t_{s,+}\,P_\nu^{-\mu}(-z) + (t_{s,-}+1)\;P_\nu^{-\mu}(z)\right]_{z=z_*}\end{aligned} \tag{2.71}$$

to leading order. Together, expressions (2.69) and (2.71) can be used to obtain a second relation between the two transmission functions $t_{s,\pm}(\lambda,\varepsilon)$, see Corollary 2.9. Thus, we can eliminate $t_{s,-}$ and obtain a leading order expression for $t_{s,+}$:

$$t_{s,+}\,\varepsilon^2\frac{\mathrm{d}z}{\mathrm{d}\chi}\frac{\mathrm{d}}{\mathrm{d}z}\left[P_\nu^{-\mu}(-z) - \frac{P_\nu^{-\mu}(-z_*)}{P_\nu^{-\mu}(z_*)}P_\nu^{-\mu}(z)\right]_{z=z_*} = \frac{\Delta_f}{\Gamma(1+\mu)} - 2\,\varepsilon^2\frac{\mathrm{d}z}{\mathrm{d}\chi}\frac{\mathrm{d}}{\mathrm{d}z}\left[\,P_\nu^{-\mu}(z)\right]_{z=z_*}$$

so that, using the Wronskian $W\left(P_\nu^{-\mu}(z), P_\nu^{-\mu}(-z)\right)(z_*)$,

$$t_{s,+} = P_\nu^{-\mu}(z_*)\frac{\frac{\Delta_f}{\Gamma(1+\mu)} - 2\,\varepsilon^2\frac{\mathrm{d}z}{\mathrm{d}\chi}\frac{\mathrm{d}}{\mathrm{d}z}\left[\,P_\nu^{-\mu}(z)\right]_{z=z_*}}{\varepsilon^2\frac{\mathrm{d}z}{\mathrm{d}\chi}W\left(P_\nu^{-\mu}(z), P_\nu^{-\mu}(-z)\right)(z_*)} \tag{2.72}$$

which, using (2.69) and (2.50), leads to the following Theorem:

Theorem 2.12. *Let $\varepsilon > 0$ be sufficiently small. The function $t_{s,+}(\lambda,\varepsilon)$ is meromorphic as a function of λ outside σ_{ess}. It has simple poles at $\lambda^{(0)}(\varepsilon)$ and $\lambda^{(2)}(\varepsilon)$ and is analytic elsewhere. The leading order behaviour of $t_{s,+}$ is given by*

$$t_{s,+}(\lambda,0) = P_\nu^{-\mu}(z_*)\frac{\frac{\sqrt{\alpha}\,z_*}{\Gamma(1+\mu)}\int_{-1}^{1}\bar{v}_{\text{in}}\,(\zeta;\lambda)\;\mathrm{d}\zeta + \frac{\mathrm{d}z}{\mathrm{d}\chi}\frac{\mathrm{d}}{\mathrm{d}z}\left[\,P_\nu^{-\mu}(z)\right]_{z=z_*}}{-\frac{1}{2}\frac{\mathrm{d}z}{\mathrm{d}\chi}W\left(P_\nu^{-\mu}(z), P_\nu^{-\mu}(-z)\right)(z_*)} \tag{2.73}$$

The nontrivial roots of the Evans function $\mathcal{D}(\lambda,\varepsilon)$ coincide with the roots of $t_{s,+}(\lambda,\varepsilon)$. These roots determine the stability of the pulse $(U_h(\xi), V_h(\xi))$.

Note that it is clear from (2.73) that $t_{s,+}$ inherits the poles of $\bar{v}_{\text{in}}$ at $\lambda = \lambda_f^{(0,2)}$.

The roots of the Evans function $\mathcal{D}(\lambda, \varepsilon)$ outside σ_{ess} are given by the roots of the product $t_{f,+}(\lambda, \varepsilon)\, t_{s,+}(\lambda, \varepsilon)$. Based on orthogonality arguments, we have established that $t_{s,+}(\lambda, 0)$ has simple poles at $\lambda = \lambda_f^{(0,2)}$, see the solvability condition (2.66). These coincide with the (simple) roots of $t_{f,+}(\lambda, 0)$ (see Lemma 2.10), so the Evans function will *not* necessarily be zero at these values of λ. Moreover, since the Evans function is analytic, this statement continues to hold for $\varepsilon > 0$. Note that $\lambda = 0$ is always a trivial eigenvalue for system (2.25), with eigenfunction $\frac{\mathrm{d}}{\mathrm{d}\xi}(U_h(\xi), V_h(\xi))$; it does not appear as a zero of $t_{s,+}(\lambda, 0)$.

2.4 Pulse stability: results

The purpose of this section is to analyse the roots of $t_{s,+}(\lambda, 0)$ as given in Theorem 2.12. The Wronskian in the denominator is always finite for $-1 < z_* < 1$ because the underlying differential equation (2.42) is only singular at $z = -1, 1$. We can therefore focus at the numerator, which is zero whenever $P_\nu^{-\mu}(z_*) = 0$ or

$$\frac{\sqrt{\alpha}\, z_*}{\Gamma(1+\mu)} \int_{-1}^{1} \bar{v}_{\text{in}}(\zeta; \lambda)\, \mathrm{d}\zeta + \frac{\mathrm{d}z}{\mathrm{d}\chi} \frac{\mathrm{d}}{\mathrm{d}z} \Big[P_\nu^{-\mu}(z) \Big]_{z=z_*} = 0 \tag{2.74}$$

Using

$$\left[\frac{\mathrm{d}z}{\mathrm{d}\chi} \right]_{z=z_*} = \frac{1}{2}(d-1)\sqrt{\alpha}(1 - z_*^2) \tag{2.75}$$

and

$$\frac{\mathrm{d}}{\mathrm{d}z} \Big[P_\nu^{-\mu}(z) \Big]_{z=z_*} = \frac{1}{1 - z_*^2} \Big((\nu - \mu) P_{\nu-1}^{-\mu}(z_*) - z_* \nu P_\nu^{-\mu}(z_*) \Big) \tag{2.76}$$

equation (2.74) can be rewritten into

$$\begin{aligned} 18\, z_*\, P_\nu^{-\mu}(z_*) \int_{-1}^{1} \int_{-1}^{\zeta} \bar{v}_+(\zeta; \lambda)\, \bar{v}_-(s; \lambda)(1 - s^2)\, \mathrm{d}s\, \mathrm{d}\zeta \\ + \frac{1}{2}(d-1) \Big((\nu - \mu) P_{\nu-1}^{-\mu}(z_*) - z_* \nu P_\nu^{-\mu}(z_*) \Big) = 0, \end{aligned} \tag{2.77}$$

using (2.70) and recalling that $\bar{u}_s(0) = \Gamma(1+\mu)\, P_\nu^{-\mu}(z_*)$ to leading order by Lemma 2.8. Since this equation is only relevant if $P_\nu^{-\mu}(z_*) \neq 0$, we divide by $z_*\, P_\nu^{-\mu}(z_*)$ (note that $z_* \neq 0$ since $u_* \neq 0$, see (2.50)) to obtain the following:

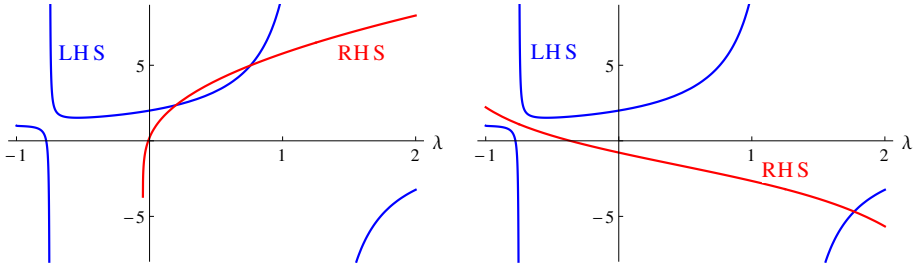

Figure 2.7: Here, LHS(λ) is plotted in blue for $\lambda \in (-1, 2)$; the red line is the graph of RHS($\frac{\lambda}{\alpha}; \nu, z_*$). In the left plot $\alpha = 0.05$, $\nu = 2$ and $z_* = 0.75$. In the right plot $\alpha = 1.5$, $\nu = 2$ and $z_* = -0.60$; the right plot is a illustration of the statement in Theorem 2.14.

Corollary 2.13. *If $P_\nu^{-\mu}(z_*) \neq 0$, the nontrivial roots of the Evans function $\mathcal{D}(\lambda, \varepsilon)$ as defined in* (2.35) *are given to leading order by the solutions of the equation*

$$18 \int_{-1}^{1} \int_{-1}^{\zeta} \bar{v}_+(\zeta; \lambda)\, \bar{v}_-(s; \lambda)(1 - s^2)\, \mathrm{d}s\, \mathrm{d}\zeta = \frac{1}{\nu - 1} \left(\nu - (\nu - \mu) \frac{P_{\nu-1}^{-\mu}(z_*)}{z_*\, P_\nu^{-\mu}(z_*)} \right), \tag{2.78}$$

with μ, ν, z_* as given in (2.43) *and* (2.50).

The left-hand side of this equation is a function of λ only; all parameters are contained in the right-hand side. Moreover, we have restricted our parameter space $(\alpha, \gamma, \sigma, d) \in \mathbb{R}_{>0} \times \mathbb{R}_{>0} \times \mathbb{R} \setminus \{0\} \times (1, \infty)$, a union of two orthants in $\mathbb{R}^4$ to $(\alpha, \nu, z_*) \in \mathbb{R}_{>0} \times (1, \infty) \times (-1, 0) \cup (0, 1)$, the union of two (semi-compact) slabs in $\mathbb{R}^3$.

It is useful to define the left- and right-hand sides of equation (2.78) separately:

$$\mathrm{LHS}(\lambda) = 18 \int_{-1}^{1} \int_{-1}^{\zeta} \bar{v}_+(\zeta; \lambda)\, \bar{v}_-(s; \lambda)(1 - s^2)\, \mathrm{d}s\, \mathrm{d}\zeta \tag{2.79}$$

$$\mathrm{RHS}(\tfrac{\lambda}{\alpha}; \nu, z_*) = \frac{1}{\nu - 1} \left(\nu - (\nu - \mu(\tfrac{\lambda}{\alpha}; \nu)) \frac{P_{\nu-1}^{-\mu(\frac{\lambda}{\alpha};\nu)}(z_*)}{z_*\, P_\nu^{-\mu(\frac{\lambda}{\alpha};\nu)}(z_*)} \right) \tag{2.80}$$

In Figure 2.7, the graphs of LHS(λ) and RHS($\frac{\lambda}{\alpha}; \nu, z_*$) are plotted for real values of λ. It is worthwhile to note that LHS(λ) = 288 $\mathcal{R}(P = \sqrt{1 + \lambda}; 2, 2)$ as used in [6].

2.4.1 Immediate results: $\sigma < 0$ and $\gamma \downarrow 0$

In this subsection we present the first 'immediate' implications of the developed theory for the stability of the pulse (U_h, V_h).

Theorem 2.14. *Let $\varepsilon > 0$ be sufficiently small. For all $\sigma < 0$, there is a real zero $\lambda_{\text{pos}} > \lambda_f^{(0)} > 0$ of the Evans function associated with the stability problem* (2.25).

Proof. As $\lambda \to \infty$, from (2.43) we infer that $\mu \gg \nu$ such that the ratio $\frac{P_{\nu-1}^{-\mu}(z_*)}{P_\nu^{-\mu}(z_*)} \to 1$. Therefore, $\text{RHS}(\frac{\lambda}{\alpha}; \nu, z_*) \rightsquigarrow \frac{\mu}{\nu-1}\frac{1}{z_*} \rightsquigarrow \frac{1}{3\sigma u_*}\sqrt{\lambda}$ as $\lambda \to \infty$. Using an equivalent argument to that in [15], Lemma 4.1 (ii), one can show that $\text{LHS}(\lambda)$ increases monotonically (from $-\infty$) to zero for $\lambda > \lambda_f^{(0)}$. Therefore, there is a $\lambda > \frac{5}{4}$ for which LHS and RHS intersect and which therefore solves (2.78) for all parameter values when $\sigma < 0$, see Figure 2.7. □

Corollary 2.15. *A pulse with a double hump in the U-component, as shown in Figure 2.1b, is always unstable.*

A direct consequence of the above Corollary is that in order to obtain any stability result, we have to confine ourselves to the interval $0 < z_* < 1$ since $\text{sgn}(z_*) = \text{sgn}(\sigma)$, see (2.50). It would be beneficial to a complete understanding of the linear stability of the constructed pulse if more would be known about the zeroes of $P_\nu^{-\mu}(z_*)$. However, while some information can be obtained regarding the number of zeroes of $P_\nu^{-\mu}(z_*)$ for real values of μ (see [1], the general case will be treated in chapter 3, section 3.5.1), the authors are not aware of any general analytic expressions concerning zeroes of $P_\nu^{-\mu}(z_*)$ for complex μ. Notwithstanding, direct numerical evaluation of $P_\nu^{-\mu}(z_*)$ for a broad parameter range has led to the following Conjecture:

Conjecture 2.16. *For all $\lambda \in \mathbb{C}$ for which $\text{Re}\,\lambda > 0$, $P_\nu^{-\mu}(z_*) \neq 0$ for all $0 < z_* < 1$. Moreover, for $\text{Im}\,\lambda \neq 0$, $P_\nu^{-\mu}(z_*) \neq 0$ for all $0 < |z_*| < 1$.*

Based on this observation, the study of linear stability of the pulse can be confined to the study of solutions of (2.78). Moreover, any additional eigenvalues originating from zeroes of $P_\nu^{-\mu}(z_*)$ would occur on the real line and be negative. Note that in the following results, this Conjecture is not needed.

Equation (2.80) can be studied for different parameter values (and limits thereof) to obtain information about the pulse spectrum. Another direct result can be obtained by taking the limit $\gamma \downarrow 0$ to remove the influence of the slow nonlinearity in (2.7) and obtain the classical Gierer-Meinhardt equations. As $\gamma \downarrow 0$, $u_* \to \frac{\sqrt{\alpha}}{3|\sigma|}$ (see (2.21)) so $z_* \to \text{sgn}(\sigma)$ using (2.50). Note that, while the limit $\gamma \downarrow 0$ reduces equation (2.7) to the 'classical' Gierer-Meinhardt equation –where the slow evolution in U is linear, yielding a 'simple' exponential instead of an associated Legendre function– the coordinate z is ill-defined for $\gamma = 0$, see (2.41) in relation to (2.40). Therefore,

some of the expressions in the following will still depend on ν, while ν disappears from (2.7) as $\gamma \downarrow 0$. Since

$$P_\nu^{-\mu}(z_*) \rightsquigarrow \frac{1}{\Gamma(1+\mu)} \left(\frac{1-z}{2}\right)^{\frac{\mu}{2}} \quad \text{as} \quad z_* \to 1 \tag{2.81a}$$

$$P_\nu^{-\mu}(z_*) \rightsquigarrow \frac{\Gamma(\mu)}{\Gamma(\mu-\nu)\Gamma(1+\mu+\nu)} \left(\frac{1+z}{2}\right)^{-\frac{\mu}{2}} \quad \text{as} \quad z_* \to -1 \tag{2.81b}$$

(see [1, 2]), this means that

$$\begin{aligned} \lim_{\gamma\downarrow 0} \mathrm{RHS}(\tfrac{\lambda}{\alpha}; \nu, z_*(\alpha,\gamma,\sigma,d)) &= \lim_{z_*\to\mathrm{sgn}(\sigma)} \mathrm{RHS}(\tfrac{\lambda}{\alpha}; \nu, z_*) = \mathrm{sgn}(\sigma)\,\frac{\mu}{\nu-1} \\ &= \mathrm{sgn}(\sigma)\sqrt{1+\frac{\lambda}{\alpha}} \end{aligned} \tag{2.82}$$

Moreover, $P_\nu^{-\mu}(z_*)$ can be written as $P_\nu^{-\mu}(z_*) = \left(\frac{1-z_*}{2}\right)^{\frac{\mu}{2}} F(z_*)$ where $F(z)$ has a regular expansion (see [1, 2]). Near $z = 1$, $F(z)$ can be expanded as $F(z) = \sum_{k=0}^{\infty} a_k \left(\frac{1-z}{2}\right)^k$, with

$$a_k = \sum_{j=0}^{\infty} \frac{\left(\frac{\mu}{2}\right)_{k-j} (-\nu)_j (\nu+1)_j}{\Gamma(1+j+\mu)(k-j)!\,j!} \tag{2.83}$$

Since $a_0 = \frac{1}{\Gamma(1+\mu)} \neq 0$ for all μ considered since $\mathrm{Re}\,\mu > 0$ and the limit $\gamma \downarrow 0$ only influences the value of z_*, it follows that $P_\nu^{-\mu}(z_*)$ does not have any zeroes asymptotically close to, but different from $z_* = 1$. The same reasoning applies for $z_* \to -1$. Therefore, in this particular limit, we do not need to appeal to Conjecture 2.16. This yields the following Lemma:

Lemma 2.17. *For $\gamma \downarrow 0$, the nontrivial pulse spectrum is to leading order given by the roots of the equation*

$$18 \int_{-1}^{1} \int_{-1}^{\zeta} \bar{v}_+(\zeta;\lambda)\,\bar{v}_-(s;\lambda)(1-s^2)\,\mathrm{d}s\,\mathrm{d}\zeta = \mathrm{sgn}(\sigma)\sqrt{1+\frac{\lambda}{\alpha}} \tag{2.84}$$

which, for $\sigma > 0$, coincides with the corresponding expression found in [6] for the classical Gierer-Meinhardt equations.

2.4.2 Varying α and investigating the role of d

As the parameter α occurs in both the expression for μ and z_* (see (2.43) and (2.50)), it is worthwhile to study the behaviour of $\mathrm{RHS}(\lambda)$ as α changes to obtain α-parametrised

eigenvalue orbits. Moreover, the parameter α is the classical parameter to be varied, as α plays the role of μ in the classical Gierer-Meinhardt equations. In Figure 2.3, left, the (complex) solutions to equation (2.78) are plotted as a function of increasing α for $d = 2$, $\gamma = 2$ and $\sigma = 1$. The eigenvalues cross the imaginary axis for $\alpha \approx 0.83083$ and converge to $\lambda \approx -0.990268 \pm 0.147318\, i$ as $\alpha \to \infty$. The same plot, now for $d = 5$, is given in Figure 2.3, middle and right. The eigenvalues initially display the same behaviour as in the case $d = 2$; here, the imaginary axis is crossed for $\alpha \approx 0.36654$. A clear change of behaviour can be seen for increasing α; whereas the orbit seems to converge to a complex conjugate pair of stable limit points for $d = 2$, for $d = 5$ the orbits crosses the imaginary axis again for $\alpha \approx 90.634$ and yields a pair of unstable eigenvalues as $\alpha \to \infty$. Note that this behaviour is essentially different from the equivalent analysis found in [6], Figure 5.3 therein.

The behaviour for $\alpha \to \infty$ can be determined explicitly: since only the right-hand side of (2.78) is parameter dependent, it suffices to calculate $\lim_{\alpha\to\infty} \mathrm{RHS}(\frac{\lambda}{\alpha}; \nu, z_*)$. Since

$$\lim_{\alpha\to\infty} \mu(\lambda; \alpha, d) = \frac{2}{d-1} = \nu - 1 \tag{2.85}$$

by (2.43) and

$$\lim_{\alpha\to\infty} z_*(\alpha, \gamma, \sigma, d) = \begin{cases} 0 & \text{if} \quad d > 3 \Leftrightarrow \nu < 2 \\ \mathrm{sgn}(\sigma) & \text{if} \quad d < 3 \Leftrightarrow \nu > 2 \end{cases} \tag{2.86}$$

by (2.21) and (2.50), we see that a dichotomy occurs at $d = 3$ or equivalently $\nu = 2$. For $\nu > 2$, the right-hand side of (2.78) converges as $\alpha \to \infty$ to

$$\lim_{\alpha\to\infty} \mathrm{RHS}\left(\tfrac{\lambda}{\alpha}; \nu > 2, z_*(\alpha)\right) = \lim_{\mu\to\nu-1} \lim_{z_*\to\mathrm{sgn}(\sigma)} \mathrm{RHS}\left(\lambda; \mu, \nu > 2, z_*\right) = \mathrm{sgn}(\sigma) \tag{2.87}$$

using (2.81).

Following the same reasoning preceding Lemma 2.17, there are no additional zeroes of $P_\nu^{-\mu}(z_*)$ to be taken into account since the same limit behaviour $z_* \to \pm 1$ takes place here. The fact that a simultaneous limit is taken for $\mu(\lambda; \alpha, d)$ does not change this, since the coefficients of the expansion of $F(z)$, given in (2.83), have a regular expansion in orders of $\frac{1}{\alpha}$. Again, $a_0 = \frac{1}{\Gamma(1+\mu)} = \frac{1}{\Gamma(\nu)} + O\left(\frac{1}{\alpha}\right)$ is not equal to zero since $\nu > 1$. Therefore, it is not necessary to appeal to Conjecture 2.16 in this limit, since again it follows that $P_\nu^{-\mu}(z_*)$ does not have any zeroes asymptotically close to, but different from $z_* = \pm 1$.

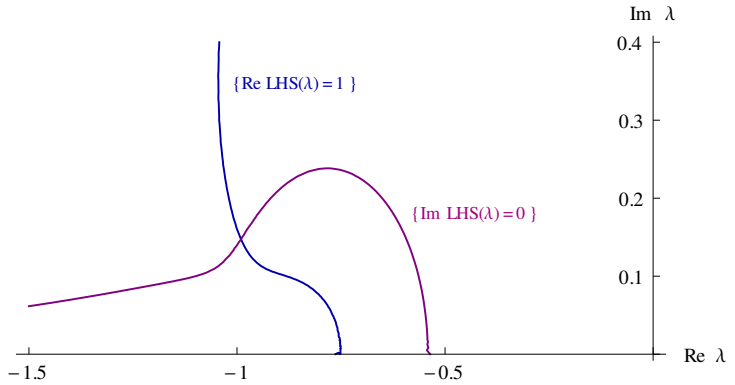

Figure 2.8: The equation $\mathrm{LHS}(\lambda) = \mathrm{sgn}(\sigma)$ is solved graphically for $\sigma > 0$. Plotted in blue is the level curve $\{\mathrm{Re}\ \mathrm{LHS}(\lambda) = 1\}$, which intersects the purple level curve $\{\mathrm{Im}\ \mathrm{LHS}(\lambda) = 0\}$ in the left half-plane for $\sigma > 0$ at $\lambda \approx -0.990268 \pm 0.147318\, i$. Since the level curves are symmetric, only the upper half-plane is shown.

The solution to $\mathrm{LHS}(\lambda) = \mathrm{sgn}(\sigma)$ is determined by direct evaluation of the integral (2.79), see Figure 2.8 for a graphic illustration. For $\sigma > 0$, this equation has a conjugate pair of complex solutions in the left half-plane; for $\sigma < 0$, there is a real positive solution, see Theorem 2.14. Of course the existence of these isolated solutions can be confirmed by a rigorous numerical winding number calculation (see [7]). Note that this both corroborates and extends the corresponding result in [6], giving a method to calculate the 'endpoints' of the eigenvalue orbits. The above leads to the following Theorem:

Theorem 2.18. *Let $\varepsilon > 0$ be sufficiently small. For all $1 < d < 3$, there is an $\alpha_*(\gamma, \sigma, d) > 0$ such that for all $\alpha > \alpha_*$, the nontrivial zeroes of the Evans function associated with the stability problem* (2.25) *are to the left of, and bounded away from the imaginary axis.*

When $\nu < 2$, we need to investigate $\lim_{z_* \to 0} \lim_{\mu \to \nu - 1} \mathrm{RHS}(\frac{\lambda}{\alpha}; \nu < 2, z_*)$. Since $P_\nu^{-(\nu-1)}(z) = z\, P_{\nu-1}^{-(\nu-1)}(z)$ [1, 2], we see that $\mathrm{RHS}(\frac{\lambda}{\alpha}; \nu < 2, z_*(\alpha)) \rightsquigarrow \frac{1}{z_*^2}$ while $z_* \to 0$ as $\alpha \to \infty$. This means that the solutions of equation (2.78) will either converge to the poles of $\mathrm{LHS}(\lambda)$, which lie at $\lambda = \lambda_f^{(2)} = -\frac{3}{4}$ and $\lambda = \lambda_f^{(0)} = \frac{5}{4}$, or take off to infinity – see Figure 2.7, right. From this, it is clear that the pulse becomes unstable for $\nu < 2 \Leftrightarrow d > 3$ when α is large enough; see again Figure 2.3 for an example.

Theorem 2.19. *Let $\varepsilon > 0$ be sufficiently small. For all $d > 3$, there are $\alpha_{*,1}(\gamma, \sigma, d) > 0$ and $\alpha_{*,2}(\gamma, \sigma, d) > 0$ such that for all $\alpha < \alpha_{*,1}$ and all $\alpha > \alpha_{*,2}$, the nontrivial zeroes of the Evans function associated with the stability problem* (2.25) *are to the right of the imaginary axis.*

Proof. The above arguments show that the pulse becomes unstable when α is large enough. For $0 < \alpha \ll 1$, we see that the same approximations apply as for the case $\lambda \to \infty$, see the proof of Theorem 2.14. Moreover, combining (2.21) and (2.50) we see that $z_* \to \operatorname{sgn}(\sigma)$ as $\alpha \downarrow 0$. Therefore, RHS $\rightsquigarrow \operatorname{sgn}(\sigma)\frac{\sqrt{\lambda}}{\sqrt{\alpha}}$ as $\alpha \downarrow 0$. As for the case $\alpha \to \infty$, RHS thus has to blow up, which yields the existence of a positive real solution close to $\lambda_f^{(0)}$ for (2.78). □

However, the eigenvalue orbit for $d > 3$ traverses the left half plane for a particular α-interval, as shown in Figure 2.3. That is, direct evaluation of (2.78) indicates that there also is a non-empty region $\alpha \in (\alpha_{*,1}, \alpha_{*,2})$ for which the pulse is stable. To investigate this behaviour analytically, we focus on the parameter d.

Consider the limit $d \gg 1$. This is equivalent with the limit $\nu - 1 \ll 1$. Therefore, we introduce an asymptotically small parameter δ and set $\nu = 1 + \delta$, so that $\mu = \delta\sqrt{1 + \frac{\lambda}{\alpha}}$ (see (2.43)). The equation for z_*, combining (2.21) and (2.50), is

$$\frac{\gamma(\nu-1)}{\nu}\left(\frac{\alpha}{9\sigma^2}\right)^{\frac{1}{\nu-1}}\left(z_*^2\right)^{\frac{1}{\nu-1}} = \alpha(1-z_*^2) \tag{2.88}$$

which, when $\nu = 1 + \delta$, yields

$$\frac{\gamma\,\delta}{1+\delta}\left(\frac{\alpha}{9\sigma^2}\right)^{\frac{1}{\delta}}\left(z_*^2\right)^{\frac{1}{\delta}} = \alpha(1-z_*^2) \tag{2.89}$$

Substituting $z_*^2 = e^{-y}$, $y > 0$, we obtain

$$\frac{\gamma\,\delta}{1+\delta}\left(\frac{\alpha}{9\sigma^2}\right)^{\frac{1}{\delta}} e^{-\frac{y}{\delta}} = \alpha(1-e^{-y}); \tag{2.90}$$

writing

$$\frac{\alpha}{9\sigma^2} = e^{\beta} \tag{2.91}$$

this becomes

$$\frac{\gamma\,\delta}{\alpha(1+\delta)}\frac{e^y}{e^y-1} = e^{\frac{y-\beta}{\delta}} \tag{2.92}$$

When $\beta > 0$, we can rewrite this as

$$y = \beta + \delta \log\left[\frac{\gamma\,\delta}{\alpha(1+\delta)}\frac{e^y}{e^y-1}\right] \tag{2.93}$$

yielding $y = \beta + \delta\log\left(\delta\frac{\gamma e^\beta}{\alpha(e^\beta-1)}\right) + \text{h.o.t.}$. When $\beta < 0$ and not asymptotically small, equation (2.92) is solved by $y = -\log\left(1-\delta\frac{\gamma}{\alpha}e^{\frac{\beta}{\delta}}\right) + \text{h.o.t.}$. This means that when $\frac{\alpha}{9\sigma^2} > 1$, then $z_*^2 = \frac{9\sigma^2}{\alpha}\left(\frac{\alpha-9\sigma^2}{\delta\gamma}\right)^\delta + \text{h.o.t}$, while $z_*^2 = 1-\delta\frac{\gamma}{\alpha}\left(\frac{\alpha}{9\sigma^2}\right)^\delta + \text{h.o.t.}$ when $\frac{\alpha}{9\sigma^2} < 1$. Thus, for $d \gg 1$ a sharp transition in the value of z_* occurs as α passes through $\alpha = 9\sigma^2$.

We will now show that at this 'transition', all zeroes of the Evans function, i.e. all solutions of (2.78) (Corollary 2.5), must have negative real part. Using the same decomposition $P_\nu^{-\mu}(z_*) = \left(\frac{1-z_*}{2}\right)^{\frac{\mu}{2}} F(z_*)$ as before, with $F(z)$ having a regular expansion near $z_* = 1$ with coefficients given by (2.83), we see that for $\mu = \delta\mu_0$, $\nu = 1+\delta$ and $z_* = 1 - \frac{1}{2}y_1\delta$ to leading order, both the term $\left(\frac{1-z_*}{2}\right)^{\frac{\mu}{2}}$ and the coefficients in (2.83) can be expanded in δ, yielding $P_{1+\delta}^{-\delta\mu_0}(1-\frac{1}{2}y_1\delta) = 1 + \frac{1}{2}\mu_0\delta\log(\delta) + O(\delta)$. From this, we can conclude that it is not possible to choose y_1 such that $P_{1+\delta}^{-\delta\mu_0}(1-\frac{1}{2}y_1\delta) = 0$ for asymptotically small δ, so Conjecture 2.16 is not needed.

First we set $\nu = 1+\delta$ in RHS (2.80):

$$\text{RHS}(\tfrac{\lambda}{\alpha}; 1+\delta, z_*) = \frac{1}{\delta}\left(1+\delta-(1+\delta-\delta\sqrt{1+\frac{\lambda}{\alpha}})\frac{P_\delta^{-\delta\sqrt{1+\frac{\lambda}{\alpha}}}(z_*)}{z_*\,P_{1+\delta}^{-\delta\sqrt{1+\frac{\lambda}{\alpha}}}(z_*)}\right) \tag{2.94}$$

The above approximations yield, with the same asymptotically small parameter δ as introduced above,

$$\text{RHS}(\tfrac{\lambda}{\alpha}; 1+\delta, z_*) = \begin{cases} -\frac{\gamma}{\alpha} + \sqrt{1+\frac{\lambda}{\alpha}} + O(\delta) & \text{if} \quad \alpha < 9\sigma^2 \\ \frac{1}{\delta}\left(1-\frac{\alpha}{9\sigma^2}\right) + 1 + \frac{-1+\sqrt{1+\frac{\lambda}{\alpha}}}{z_*^3} + O(\delta) & \text{if} \quad \alpha > 9\sigma^2 \end{cases} \tag{2.95}$$

From this result, we see that for $\alpha < 9\sigma^2$, the behaviour of RHS is similar to the behaviour treated in Theorem 2.18. Moreover, for $\gamma \downarrow 0$, we obtain the same result as in Lemma 2.17.

However, when α crosses the threshold $\alpha \approx 9\sigma^2$, the behaviour of RHS radically changes. This accounts for the sharp 'turning' behaviour observed in Figure 2.3b. The expression for $\alpha > 9\sigma^2$ only accounts for the limiting behaviour yielding unstable eigenvalues as described in Theorem 2.19, since RHS blows up: to study the intermediate regime, we must zoom in on the situation when $\alpha \approx 9\sigma^2$. By (2.91), we thus set $\beta = \delta B + \text{h.o.t.}$, we see that equation (2.92) can be solved by $y = \delta y_1 + \text{h.o.t.}$, with y_1 determined by

$$\frac{\gamma}{\alpha} e^B = y_1 e^{y_1} \tag{2.96}$$

so $y_1 = W(\frac{\gamma}{\alpha} e^B)$, where $W(z)$ is the Lambert W-function. Since $z_*^2 = e^{-y} = 1 - \delta y_1$ at leading order, the same approximation as for $\alpha < 9\sigma^2$ can be used, yielding

$$\text{RHS}(\tfrac{\lambda}{\alpha}; 1+\delta, z_*) = -B + \sqrt{1 + \frac{\lambda}{\alpha}} + \text{h.o.t.} \quad \text{if} \quad \frac{\alpha}{9\sigma^2} = 1 + \delta B + O(\delta^2) \tag{2.97}$$

Using the previous analysis, we can go beyond the previous instability result for $d > 3$ and find an interval for α where the pulse is stable, and state the following:

Theorem 2.20. *Let $\varepsilon > 0$ be sufficiently small. There is a $d_* > 3$ such that for all $d > d_*$, there is an open set Ω_* in (α, γ, σ)-parameter space such that for all $(\alpha, \gamma, \sigma) \in \Omega_*$, the nontrivial zeroes of the Evans function associated with the stability problem* (2.25) *are to the left of, and bounded away from the imaginary axis.*

Proof. For $d \gg 1$, the above analysis can be applied. Taking $\alpha = 9\sigma^2$, we obtain from (2.97) $\text{RHS}(\frac{\lambda}{\alpha}) = \sqrt{1 + \frac{\lambda}{\alpha}}$ as a leading order expression for RHS. Taking $\sigma = 1$, solving $\text{LHS}(\lambda) = \sqrt{1 + \frac{\lambda}{\alpha}}$ numerically yields $\text{Re}\,\lambda = -1.2 < 0$ for these parameter values. Note that in this asymptotic approximation, the value of γ does not play a role. Therefore, for fixed $\gamma = \gamma_*$, there is a $d \gg 1$ such that there is an open neighbourhood of $(\alpha, \gamma, \sigma) = (9, \gamma_*, 1)$ where the statement of the Theorem holds. As observed above, since this only concerns the numerical evaluation of a meromorphic, coefficient free expression, this result can be confirmed rigorously by a winding number calculation. □

For fixed values of the parameter d, accurate numerical simulations and rigorous numerical winding number calculations similar to those used in the proof of the main stability theorem in [7] can be used. For $(\alpha, \gamma, \sigma) = (\frac{1}{2}, 2, 1)$, such numerical calculations show that for d between 3 and 21, there is a pair of complex conjugate eigenvalues with real part < -0.02, where the real part decreases as d increases. Based on these numerical calculations, we believe Theorem 2.20 holds for all $d > 3$.

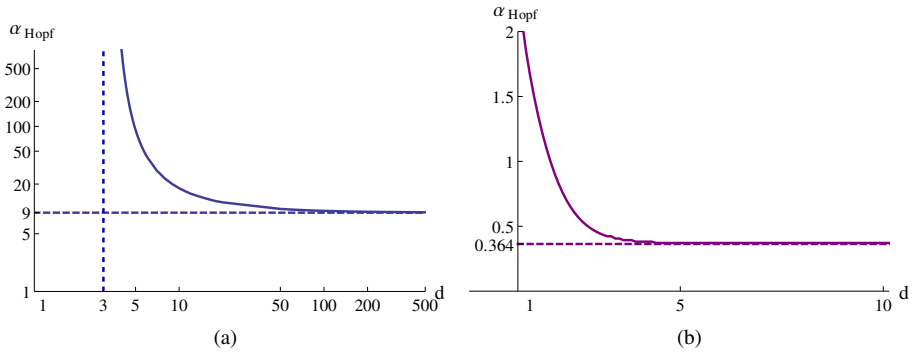

Figure 2.9: The stabilising (a) and destabilising (b) Hopf bifurcation values α_{Hopf} as a function of d.

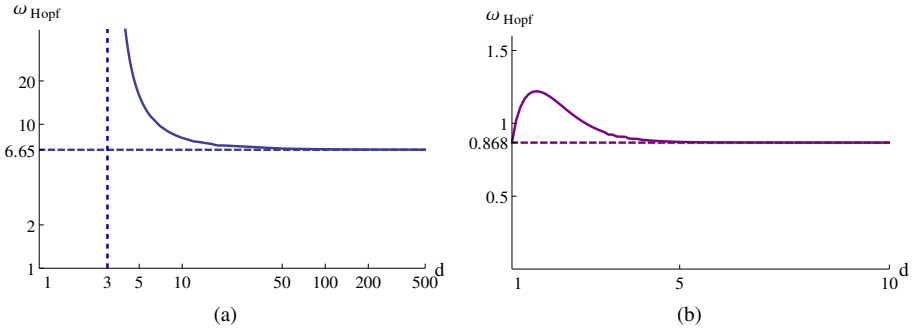

Figure 2.10: The stabilising (a) and destabilising (b) Hopf frequencies ω_{Hopf} as a function of d.

2.5 Numerical simulations

A Hopf bifurcation occurs when the eigenvalues cross the imaginary axis; this happens once for $d < 3$ (see Figure 2.3a) and twice for $d > 3$ (see Figure 2.3b). A plot of the bifurcation value α_{Hopf} as a function of d for both stabilising and destabilising Hopf bifurcations is given in Figure 2.9 for $\gamma = 2$ and $\sigma = 1$. The Hopf frequency $\omega_{\text{Hopf}} = \text{Im}\,\lambda_{\text{Hopf}}$ for both Hopf bifurcations as a function of d is given in Figure 2.10; again, $\gamma = 2$ and $\sigma = 1$. As the destabilising Hopf bifurcation only occurs for $d > 3$, a vertical asymptote at $d = 3$ can be found at both Figures 2.9b and 2.10b. For large

values of d, the functions seem to converge to the indicated horizontal asymptotes. Based on the asymptotic $d \gg 1$ analysis of the previous subsection, the asymptote $\lim_{d\to\infty} \alpha_{\text{Hopf}} = 9$ of Figure 2.9b can be understood by looking at the asymptotic expansion of RHS for $\nu = 1 + \delta$, see (2.95). If α crosses the threshold $\alpha = 9\sigma^2$, RHS blows up yielding unstable eigenvalues, in a manner equivalent to the situation described in Theorem 2.14. Since RHS blows up for asymptotically small δ, the unstable regime lies asymptotically close to $\alpha = 9\sigma^2$, which explains the horizontal asymptote $\alpha_{\text{Hopf}} = 9$ in Figure 2.9b.

The super- or subcriticality of both stabilising and destabilising Hopf bifurcations has been checked by direct numerical simulation of the constructed pulse. The pulse was simulated on the domain $x \in [-10\,\varepsilon^{-1}, 10\,\varepsilon^{-1}]$ with homogeneous Neumann boundary conditions. Note that in all these direct numerical pulse simulations, the position of the pulse was seen to remain completely fixed. This phenomenon will be treated in detail in chapter 4, section 4.3.2.
In Figure 2.11, the tip of the U-component of the simulated pulse is plotted as a function of time for $d = 2$. Here, $\gamma = 2$, $\sigma = 1$ and $\varepsilon = 0.02$. For these parameter values, the Hopf bifurcations occurs at $\alpha_{\text{Hopf}} = 0.83 + O(\varepsilon)$. Figure 2.11 shows that for these parameter values, the Hopf bifurcation is subcritical. For $d = 5$, the equivalent stabilising Hopf bifurcation occurs at $\alpha_{\text{Hopf}} = 0.37 + O(\varepsilon)$ for the same values of the other parameters. As can be seen in Figure 2.12, this Hopf bifurcation is subcritical as well.

The destabilising Hopf bifurcation occurs for $d = 5$ at $\alpha_{\text{Hopf}} = 90.634 + O(\varepsilon)$. In this simulation, $\varepsilon = 0.002$ while still $\gamma = 2$ and $\sigma = 1$. In Figure 2.13 it can be seen that upon destabilisation, the pulse tip initially exhibits typical 'subcritical' growth behaviour. However, for longer times, a bounded temporally oscillating pulse is observed. Nearby the other Hopf bifurcations, such 'breathing' pulses can also be observed. For $d = 2$ and stable values of α, i.e. for α within the region in which the pulse is stable (here, $\alpha = 0.9 > \alpha_{\text{Hopf}}$), Figure 2.14 shows an oscillating pulse.

In Figures 2.15, 2.16 and 2.2, the oscillating behaviour of the pulse near the destabilising Hopf bifurcation for $d = 5$ is studied in more detail. For parameter values relatively far in the stable regime (here, $\alpha = 85 < \alpha_{\text{Hopf}} = 90.634 + O(\varepsilon)$), simulations reveal bounded temporally periodic behaviour with a slowly periodically modulated amplitude, see Figure 2.15. When α is increased towards α_{Hopf}, the frequency of the modulation increases; see Figure 2.16 for the pulse behaviour when $\alpha = 90.5$. For parameter values even closer to α_{Hopf}, the irregular behaviour as shown in Figure 2.2 is observed.

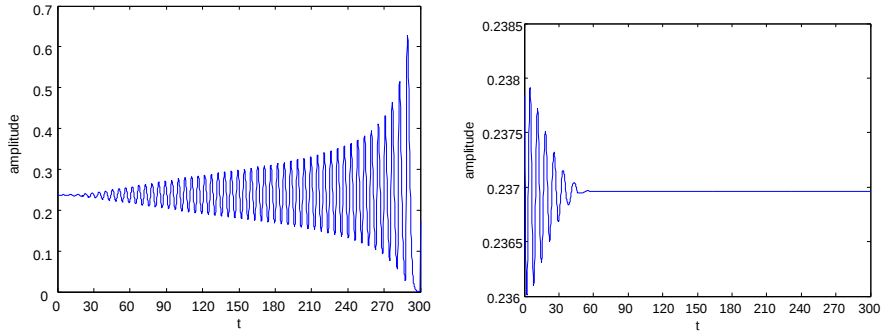

(a) (b)

Figure 2.11: The tip of the U-pulse as a function of time for $\alpha = 0.827$ (a) and $\alpha = 0.829$ (b). Here, $d = 2$.

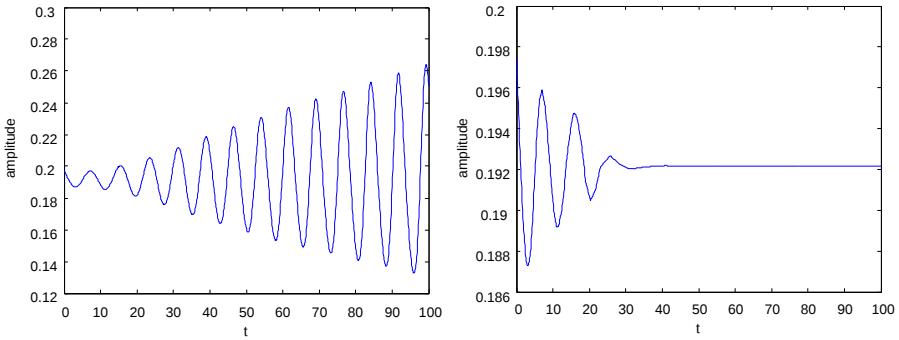

(a) (b)

Figure 2.12: The tip of the U-pulse as a function of time for $\alpha = 0.352$ (a) and $\alpha = 0.353$ (b). Here, $d = 5$.

This pulse behaviour has not been observed in the literature on GS/GM-type models. In the fourth chapter of this thesis, the nature of the Hopf bifurcation of pulses in system (2.7) is studied. It is established that this Hopf bifurcation can be both sub- and supercritical, see chapter 4, Theorem 4.16.

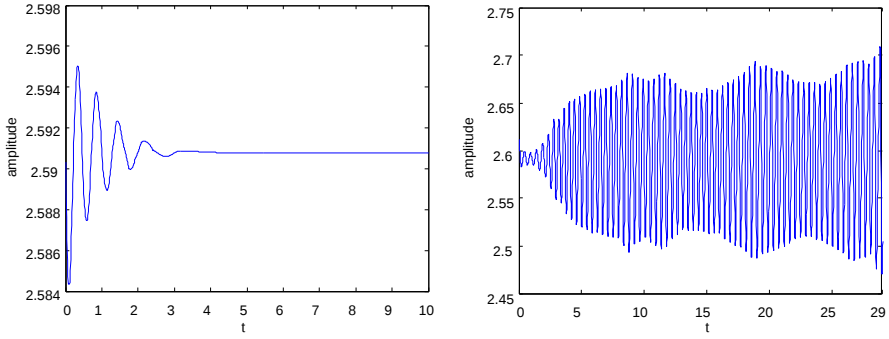

(a) (b)

Figure 2.13: The tip of the U-pulse as a function of time for $\alpha = 90.61$ (a) and $\alpha = 90.69$ (b).

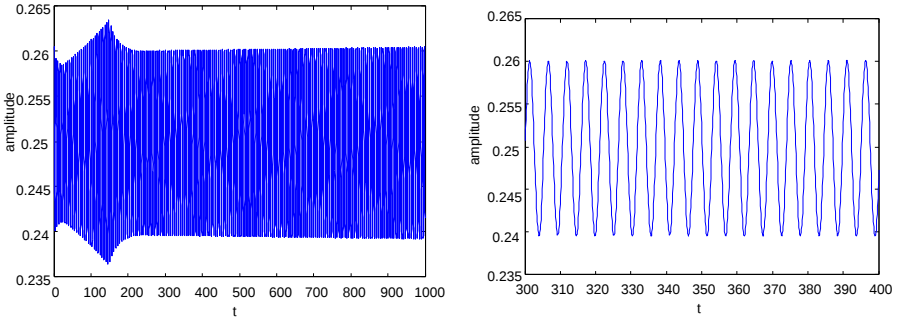

(a) (b)

Figure 2.14: The tip of the U-pulse as a function of time for $\alpha = 0.9$, $d = 2$. Figure (a) shows the entire simulated time domain, while (b) zooms in on a part of the time domain, showing the regularity of the pulse tip movement.

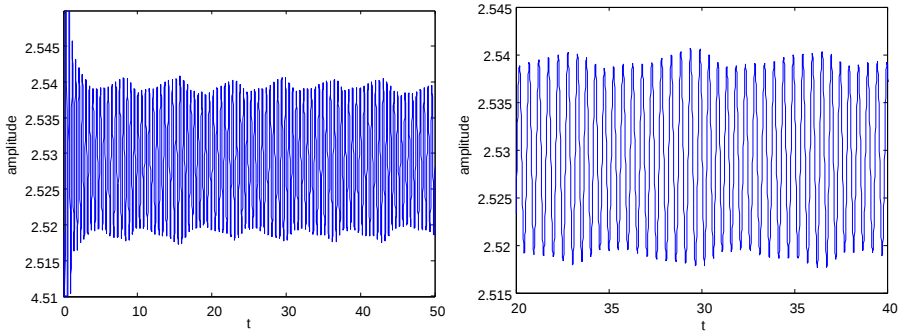

(a) (b)

Figure 2.15: The tip of the U-pulse as a function of time for $\alpha = 85$, $d = 5$. Figure (a) shows the entire simulated time domain, while (b) zooms in on a part of the time domain.

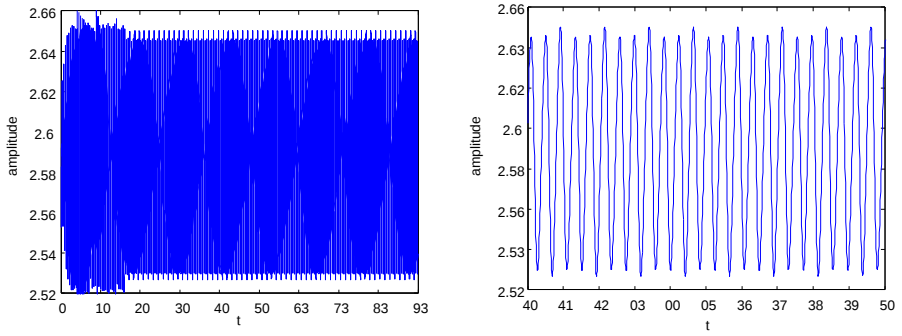

(a) (b)

Figure 2.16: The tip of the U-pulse as a function of time for $\alpha = 90.5$, $d = 5$. Figure (a) shows the entire simulated time domain, while (b) zooms in on a part of the time domain.